CO4-1 Study on HPLC Elution Behavior of Heavy Lanthanide Metalloufullerenes

K. Akiyama[1], D. Nakamura[1], T. Kuroda[1], K. Takamiya[2], and S. Kubuki[1]

[1]*Department of Chemistry, Tokyo Metropolitan Univer-sity*
[2]*Institute for Integrated Radiation and Nuclear Science, Kyoto University*

INTRODUCTION: Metallofullerene (EMF) is a clathrate compound encapsulating metal atom in fullerene molecule. Lanthanide (Ln) EMFs: Ln@C_{82} have two or three charge transferred electrons on the C_{82} cage from the encapsulated Ln atom, and their electronic states reflecting the number of charge transfer electrons [1]. From the view point of inorganic chemistry, It is interesting to know that the effect of the electronic state for a series of the encapsulated 10 lanthanide elements (La, Ce, Pr, Nd, Gd, Tb, Dy, Ho, Er, Lu) with the electronic states of (Ln^{3+})@(C_{82}^{3-}) on the electronic state of the Ln@C_{82} molecule from the difference in interaction with pylenyl stationary phase. So far, we have made clear the retention time in the pyrenyl stationary phase for five types of Ln@C_{82} from La to Gd by the thermal neutron activation method. On the other hand, the high-performance liquid chromatography (HPLC) retention time of Ln@C_{82} with heavy lanthanide elements have not been obtained because the half-life of the radio nuclide produced by thermal neutron irradiation such as Dy and Er is very short, and the interference by the production of Ln_2@C_{82} and Ln_2C_2@C_{80}, whose production rate increase competitively with Ln@C_{82} as the increase of the atomic number of Ln. In previous work, we used already purified Ln@C_{82} of heavy lanthanide by HPLC column of a 5PBB for the neutron activation and developed at three different temperature using newly developed column cooler to obtained detailed HPLC retention time of these Ln@C_{82}s and successively evaluated the adsorption-desorption enthalpy (ΔH) at room temperature (RT), 0 ºC, and -10 ºC for Ln@C_{82} of La, Ce, Pr, Tb, Dy, Ho, and Er on a pyrenyl stationary phase [2]. However, obtained HPLC retention time and evaluated ΔH for Ce and Tb were slightly larger than that for other lanthanide considering about the similarity of chemical properties of lanthanide elements. In the previous experiment, we had to develop Ln@C_{82} for short half-life (La, Pr, Dy, Ho, and Er) and long half-life radioisotopes (Ce and Tb) by HPLC separately due to the limitation of the half-life. In this time, we used HPLC-separated samples of mixed Ln@C_{82} solution regardless of their half-lives as irradiated samples in order to confirm the reproducibility of the retention times previously obtained.

EXPERIMENTS: Already isolated La@C_{82}, Tb@C_{82} and Dy@C_{82} were dissolved in toluene and mixed to prepare samples for HPLC development. These samples were injected into a Buckyprep column and the eluate was fractionated every 20 seconds at RT and every 1 minute at -10 ºC. These fractionated eluates were evaporated to dryness and re-dissolved to carbon disulfide and then dropped onto paper filters with 12 mm diameters and dried. These samples were sealed into polyethylene bags and irradiated in ethylene vial and activated by a thermal neutron in the KUR of the Institute for Integrated Radiation and Nuclear Science, Kyoto university. After the irradiation, the g rays emitted from the samples were measured by a Ge detector.

RESULTS: Figure 1 show HPLC elution behavior of Ln@C_{82}s studied in this work obtained at room temperature and -10 ºC. HPLC retention time (t_R) of these Ln@C_{82} were evaluated from the least square fitting with extreme function and determined as 60.41, 62.41, and 61.36 for La, Tb, and Dy at RT and 86.53, 90.24, and 88.58 for La, Tb, and Dy at -10 ºC, respectively. The separation coefficient (α) of Tb@C_{82} and Dy@C_{82} to La@C_{82} were evaluated from obtained t_R and $\alpha_{Tb@C82}$ at -10 oC was found to be quite smaller than that obtained in previous work. From these results, it was clarified that the retention time of Tb@C_{82} at -10 ºC obtained in the previous study was overestimated, as well as that of Ce determined using long half-life nuclides.

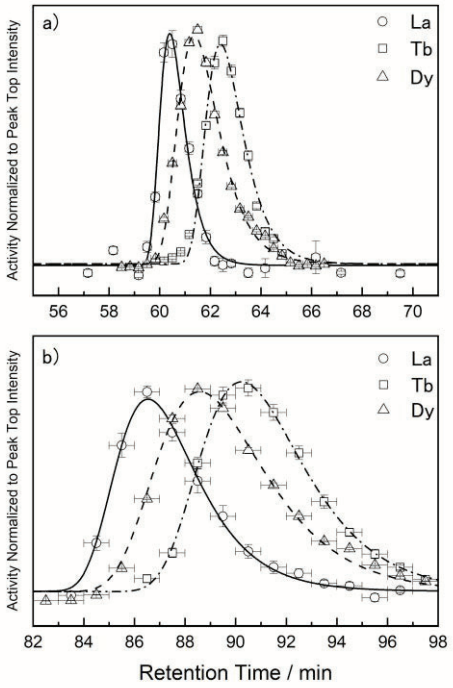

Fig. 1. HPLC elution behavior of Ln@C_{82}s studied in this work obtained at a) room temperature and b).

REFERENCES:

[1] H. Shinohara, Rep. Prog. Phys., **63** (2000) 843-892.
[2] K. Akiyama *et al*., KURNS Prog. Rep. 2021, CO4-20.

CO4-2 Radiation Tolerance of SiC p+n Junction-Diodes for High-Energy Physics Experiments

T. Kishishita, H. Yashima[1], R. Kosugi[2]

High Energy Accelerator Research Organization, KEK
[1] Institute for Integrated Radiation and Nuclear Science, Kyoto University
[2] National Institute of Advanced Industrial Science and Technology

INTRODUCTION: Silicon carbide (SiC) has been considered as a potential alternative to Si for the manufacture of dosimeters, spectrometers, and charge particle detectors in high energy physics experiments, by virtue of its operation capability in strong radiation and/or high-temperature environments. To take advantage of such properties for future radiation detectors with a comparable size of silicon, we investigated the influence of the bulk defects on the radiation sensor characteristics under the reverse-bias condition, by irradiating neutrons at Institute for Integrated Radiation and Nuclear Science, Kyoto University.

EXPERIMENTS: The reverse blocking characteristics and leakage current characteristic are primary concerns of the radiation effects. The radiation-induced effects are generally divided into bulk and surface defects. The formers are caused by the displacement of crystal atoms, introducing to the increase of the leakage current and degraded reverse blocking characteristics. The latter include all effects in the covering dielectrics and the interface region. Since the bulk damage caused by the elastic nuclear scattering of the lattice nuclei has a profound effect in our device, we irradiated fast neutrons to SiC pn-diodes under the bias condition of 1 kV [1]. The irradiation test was conducted at KUR. Fig. 1 shows the photograph of the measurement setup. We installed two SiC sensors at the front of the rail-instrument. After the 1MW operation, we carried out measurements of the leakage current and compared with those of the pre-irradiation samples.

RESULTS: The typical I-V characteristics before irradiation is shown in Figure 2. The data before the irradiation are plotted in white and black, while those after the irradiation are shown in colors. We note that the data around 1 kV are overlapped and the leakage current characteristics is not changed in the irradiation. The reverse blocking property was also retained up to 1 kV, which is required for full depletion of the SiC devices. Irradiation tests at higher fluences are performed in FY-2023. We note that the 1 MeV neutrons have the same efficiency in the detector degradation as 24 GeV protons at a comparable neutron equivalent fluence. The theoretical nonionizing energy loss (NIEL) calculation performed on SiC can be found in Lee et al. [2]. The primary radiation defects produced by single particles (protons and pions) or gamma-rays were not evaluated in this measurement, however, the number of primary defects is reported as low as that of diamond. Thus, we conclude that the bulk defects introduced by irradiation at the 10^{12} neutron equivalent fluence is ignorable, even with the reverse bias of 1 kV.

Fig. 1. Photograph of the measurement setup.

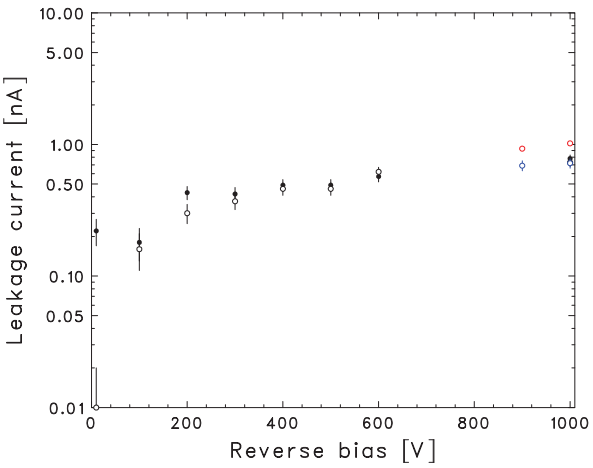

Fig. 2. Leakage currents before (plotted in white and black) and after (plotted in colors) 1 MeV neutron irradiation of 10^{12} n_{eq}/cm^2.

REFERENCES:

[1] T. Kishishita *et al.,* IEEE Trans. Nucl. Sci., **68** (2020) 2787-2793.
[2] K. K. Lee *et al.,* Nucl. Instrum. Methods Phys. Res. B, **210** (2003) 489-494.

CO4-3 Positron Annihilation Spectroscopy in Neutron-irradiated Fe-Cr Alloys

K. Sato, Y. Noshita, R. Kasada[1], Q. Xu[2], A. Yabuuchi[2], A. Kinomura[2]

Graduate School of Science and Engineering, Kagoshima University
[1]Institure for Materials Research, Tohoku University
[2]Institute for Integrated Radiation and Nuclear Science, Kyoto University

INTRODUCTION: Ferritic stainless and heat resistant steels used as nuclear reactor peripheral materials have high Cr content [1]. In these materials, ductility and toughness remarkably decrease, and hardness and tensile strength increase by aging from 593 to 813 K. This phenomenon is caused by the formation of Fe-rich and Cr-rich phase, and is called 475˚C embrittlement [2]. These changes in mechanical properties are an important issue in terms of evaluation of aged deterioration when it was used as a reactor structural material. The phase separation process of Fe-Cr binary alloys have studied by the small angle neutron scattering method [3], Mossbauer spectroscopy [4] and atom probe field ion microscopy [5] etc. Chen et al. detected phase separation in Fe-9.7%Cr irradiated with neutrons at 573 K by atom probe tomography [6], and reported that irradiation-induced excessive defects promote phase separation even at a temperature of less than 593 K.

Positron annihilation spectroscopy (PAS) is very powerful tool to obtain the information of vacancy-type defects (even single vacancies) and precipitates. Xu et al. reported the positron annihilation lifetimes of vacancy clusters and the change in spectra of coincidence Doppler broadening (CDB) in association with the formation of Cu precipitates in neutron-irradiated Fe-Cu alloys [7]. In Fe-Cu alloys, positron affinity of Cu is lower than that of Fe [8], and the formation of Cu precipitates leads to the change in spectra of CDB. In Fe-Cr alloys used in this study, positron affinity of Fe is lower than that of Cr [8]. Therefore, we can detect the formation of Fe-rich phase in phase separation of Fe-Cr alloys using PAS. The purpose of this study is to detect the progress of phase separation using PAS, and to obtain the correlation between the hardness and phase separation in Fe-Cr binary alloys irradiated with neutrons at 473K and 573 K.

EXPERIMENTS: Fe-x wt.%Cr (x = 0, 9, 15, 30, 45, 50, 70, 85, 91, and 100) binary alloys were used in this study. The weight of high purity Fe (99.99%) and Cr (99.99%) were measured, and samples were melted by the arc melting. For neutron irradiation, samples with diameters of 3 mm and thickness of 0.25 mm were cut using the wire electric discharge machine. Fe-xCr (x = 30, 45, 50, 70, 85, 91, and 100) were annealed at 1273K for 1h, and Fe-xCr (x = 0, 9, 15) were annealed at 1073K for 1h in a vacuum (< 4×10^{-4} Pa), and then water-quenching was performed for the suppression of phase separation. The neutron irradiation was carried out at the Material Controlled Irradiation Facility (SSS) of Kyoto University Reactor (KUR) [9]. The irradiation doses were 0.44×10^{-3} , 0.5×10^{-3} and 2.1×10^{-3} dpa. The irradiation temperature was 473K (0.5×10^{-3} dpa) and 573K (0.44×10^{-3} and 2.1×10^{-3} dpa). All samples were electropolished after neutron irradiation to remove the oxidation layers. Measurements of positron annihilation lifetime (PAL) were performed at room temperature. The PAL spectrometer had a time resolution of 190 ps (full width at half maximum) and each spectrum was accumulated to a total of 4×10^{6} counts. PAL spectra were analyzed using PALSfit package [10].

RESULTS: Vacancy clusters consisting of 8−12 vacancies were formed in the 473 K irradiation expect for Fe-70Cr, Fe-85Cr, Fe-91Cr. Larger vacancy clusters were detected in pure Fe and Cr. In pure metals, because the solute atoms, which suppress the migration of vacancies, do not exist, vacancy clusters are larger than in alloys. In the 573 K irradiation, no vacancy clusters were observed expect for pure Cr. Yoshiie et al. reported that the density of vacancy clusters in pure Fe irradiated with neutrons at 473 K was higher than that at 573 K from the results of PAL measurements. They also indicated that the low density of vacancy clusters was detected in the irradiation at 573 K at a dose of 2.1×10^{-2} dpa [11]. In this study, the irradiation doses were so low that we could not detect vacancy clusters in the 573 K irradiation. In the next step, we will discuss why we cannot detect vacancy clusters in Fe-70Cr, Fe-85Cr and Fe-91Cr irradiated at 473 K.

REFERENCES:

[1] R.L. Klueh *et al.,* J. Nucl. Mater., **191** (1992) 116.
[2] R.O. Williams, Trans. AIME, **212** (1958) 497.
[3] M.H. Mathon *et al.,* J. Nucl. Mater., **312** (2003) 236.
[4] H. Kuwano *et al.,* J. Japan Inst. Metals, **45** (1981) 457.
[5] S.S. Brenner *et al.,* Scripta Metall., **16** (1982) 831.
[6] W.Y. Chen *et al.,* J. Nucl. Mater., **462** (2015) 242.
[7] Q. Xu *et al.,* Philos. Mag. Lett., **88** (2008) 353.
[8] M. J. Puska *et al.,* J. Phy. Condes. Matter, **1** (1989) 6086.
[9] T. Yoshiie *et al.,* Nucl. Instr. Meth. Phys. Res. A, **498** (2003) 522.
[10] J.V. Olsen *et al.,* Phys. Stat. Sol., **C4** (2007) 4004.
[11] T. Yoshiie *et al.,* J.Nucl.Mater., **325**(2007) 367-370.

CO4-4 The change of free volume in highly-hydrogenated DLC film due to thermal desorption

K. Kanda, D. Niwa, T. Inoue, F. Hori[1], A. Yabuuchi[2] and A. Kinomura[2]

Laboratory of Advanced Science and Technology for Industry, University of Hyogo
[1]Osaka Metropolitan University
[2]Institute for Integrated Radiation and Nuclear Science, Kyoto University

INTRODUCTION: Highly-hydrogenated diamond-like carbon (H-DLC) films containing more than 40% hydrogen have been reported to take a low coefficient of friction even in a vacuum and are expected to be used as lubricants for use in a vacuum [1]. In order to use H-DLC film as a lubricant, it is necessary to know its temperature characteristics. We have performed thermal desorption spectrometry (TDS) measurements on H-DLC films and observed that hydrogen desorption occurs around 360°C and hydrocarbon desorption around 400-450°C. In this experiment, we used PAS to measure how the free volume in the highly-hydrogenated DLC films changes with increasing temperature.

EXPERIMENTS: H-DLC film was deposited on Si wafers by using an amplitude-modulated radio-frequency plasma-enhanced chemical vapor deposition method. (Nippon ITF Co.) The desired film thickness was 200-nm-thick. The hydrogen content of H-DLC film was estimated to be ≈50 at.%.

The temperature of the H-DLC films was raised in an electric furnace of the TDS system. The vacuum before the temperature increase was 5.5×10^{-5} Pa, and the temperature increase rate was 5°C/min. These were the same condition as the TDS measurements. Samples were prepared by stopping the temperature increase at 200, 360, 400, 450, 550, and 700°C. After the temperature was raised, the samples were cooled naturally in a vacuum and then removed from the furnace and stored in a dry box.

Positron lifetime spectroscopy (PAS) measurement was performed at the slow positron beam system (B-1) at Kyoto University research Reactor (KUR). Doppler broadening profiles of annihilation γ-rays were obtained using a Ge detector for each positron energy. The low and high momentum parts of spectra were characterized by the *S* and *W* parameters. *S* and *W* parameters as a function of energy were measured in the range of 0 - 30 keV. Positron annihilation lifetime spectroscopy (PALS) was performed at an energy of 2 keV, corresponding to the DLC film on Si. A Kapton (polyimide) film was measured before and after measurements of the DLC samples as a control sample. Obtained lifetime spectra were analyzed by the PALSfit code assuming one-lifetime component.

RESULTS: Figure 1 shows the temperature-dependence of positron annihilation lifetime (PAL) and the *S* parameter. The film thickness decreased due to desorption of species from the H-film as the temperature rose. Therefore, we could only measure PAL up to a sample with a temperature rise of 360°C. The *S* parameter of the H-DLC film before temperature rise was ≈0.484 and it increased to ≈0.488 by temperature rise to 200°C. The *S* parameter showed no significant change in temperature range from 200°C to 400°C, followed by a sharp increase to 450°C. The *S* parameter kept ≈0.497 in the temperature range above 450°C. On the other hand, the PAL of the H-DLC film before temperature rise was 0.382 ns and it increased to 0.415 ns by temperature rise to 360 °C.

In the TDS spectrum of H-DLC film, desorption of endohedral gas, which was the source gas left in the film during film deposition, was observed at ≈200°C. The increases in the *S* parameter and PAL of the H-DLC film at 200°C is thought to be due to the increase in free volume resulting from desorption of the endohedral gas.

Hydrogen desorbed from DLC at around 360°C in TDS measurements. The increase in PAL between 200°C and 360°C can be attributed to the increase in free volume in the H-DLC film due to hydrogen desorption from carbon skeleton of DLC. On the other hand, the *S* parameter did not increase in this temperature range. This is due to the fact that the free-volume periphery has changed from hydrogen, which has only valence electrons, to carbon, which has inner-shell electrons.

Desorption of hydrocarbons - i.e., destruction of the carbon skeleton - was observed near 450°C in the TDS spectrum. The steep increase in the *S* parameter from 400 to 450°C is thought to be due to the increase in free volume resulting from desorption of the hydrocarbons. In this temperature range, graphitization of the film proceeded rapidly, and at higher temperatures the film thickness gradually decreased due to desorption.

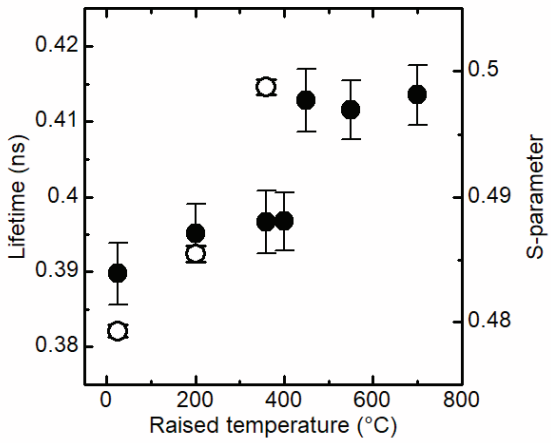

Fig. 1. The temperature-dependence of positron annihilation life-time (○) and the *S* parameter (●).

REFERENCES:

[1] C. Donnet *et al*., Surf. Coatings Technol., **68-69** (1994) 626–631.

CO4-5 Effect of gamma radiation on ultra-micro structure of hardwood cell-wall

K. Murata, Y. Imataki, M. Nakamura, T. Saito[1]

Graduate School of Agriculture, Kyoto University
[1]Institute for Integrated Radiation and Nuclear Science, Kyoto University

INTRODUCTION: Space-wood project (LignoStella project) is performed by Kyoto University collaborating with Sumitomo forestry Co Ltd in order to challenge to use wood-material in outer space. Firstly, possibility to use wood material in outer space has to be confirmed because a small wooden artificial satellite is going to launch until 2023. Space exposure test of wood specimen started on ExBAS at ISS in March 4, 2022. The wood specimen was exposed for about 1 year and came back to Earth in March, 2023. They were affected by atomic oxygen and cosmic ray. In this study, effect of gamma-ray irradiation on cell-wall of wood material was studied on the ground in parallel with the exposure tests in outer space.

EXPERIMENTS: The sample was Honoki (*Magnolia obovate*), which is 100 mm (length) ×10 mm (radial) × 0.6 mm (tangential) in size. They were conditioned in 20 °C and 60%RH (dry wood) or 20℃ and 97%H (wet wood) for a few weeks before the doze test. They were wrapped in polyethylene film to prevent moisture content changes during irradiation. They were irradiated for 24 hours, and five types of doze was performed, which is 50 kGy, 16 kGy, 10 kGy, 4 kGy adn 1 kGy. After irradiation, ultra-micro structure of cell wall was observed using a Wide-Angle X-Ray Diffraction (WAXD) (Shimadzu, XRD-7000s). X-ray diffraction (wave length 0.154 nm) was measured under the conditions that the scan speed is 1°/min and the sampling width is 0.02°, and scanning range is 2θ=10~30°. Crystallite size or the degree of crystallinity were measured using diffraction profiles.

RESULTS: As shown in Fig. 1 and Fig. 2, the degree of crystallinity were obtained using integral intensity values of crystalline and non-crystalline peaks. They did not change by irradiation. Aoki *et al*. [1] state that the degree of crystallinity of wood remained almost unchanged up to 300 kGy of gamma rays doze, but started to decrease rapidly at about 1000 kGy. This result corresponds with that of Aoki *et al*. As shown in Fig. 3 and Fig. 4, crystallite size was obtained using Scherrer's equation. The size was identified as diameter of cellulose micro fibril (CMF), so we consider that the WAXD measurement results is appropriate. In the case of dry wood, diameters of CMF increased slightly by 50 kGy irradiation (statistically significant differences, based on t-test, $p < 0.050$). We believe that this may be due to the decomposition of the hemicellulose surrounding CMF by high-dose irradiation, but we need to consider about this reason.

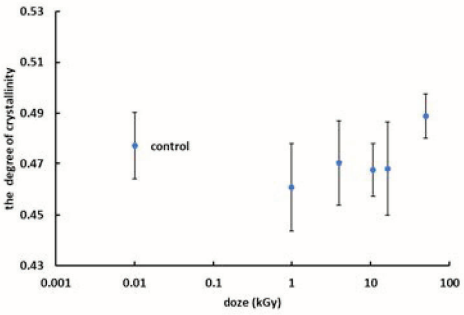

Fig. 1. Change of the degree of crystallinity of wet wood by gamma irradiation.

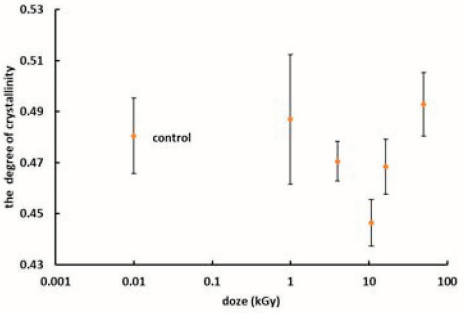

Fig. 2. Change of the degree of crystallinity of dry wood by gamma irradiation.

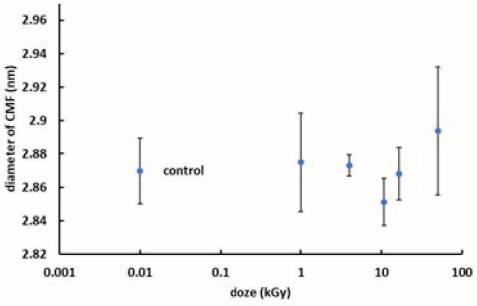

Fig. 3. Change of diameter of CMF of wet wood by gamma irradiation.

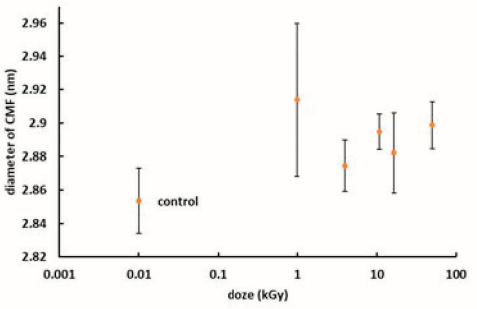

Fig. 4. Change of diameter of CMF of dry wood by gamma irradiation.

REFERENCES:

[1] T. Aoki *et al.*, bulletin of the Wood Research Institute Kyoto Univ. **62** (1977) 19-28.

CO4-6 Investigation of Concentration Dependence on Local Structures at Cd Sites in $Cd_xSr_{1-x}TiO_3$

S. Komatsuda, W. Sato[1], A. Taniguchi[2], M. Tanigaki[2], and Y. Ohkubo[2]

Institute of Human and Social Sciences, Kanazawa University
[1]*Institute of Science and Engineering, Kanazawa University*
[2]*Institute for Integrated Radiation and Nuclear Science, Kyoto University*

INTRODUCTION: Strontium titanate ($SrTiO_3$) is a cubic perovskite compound of ABO_3 type. Among ABO_3 perovskites, $SrTiO_3$ has a wide band gap values of 3.2 eV, and doping effect of $SrTiO_3$-based materials is attracting much attention. It is known from many previous reports that chemical and physical properties of $SrTiO_3$ change depending on the kind of dopant ions and the surrounding local structures[1]. For a practical use of $SrTiO_3$, it is necessary to obtain microscopic information on various impurity sites. Therefore, we applied the time-differential perturbed angular correlation (TDPAC) method to study the local structures at impurity sites in $SrTiO_3$. In our previous TDPAC study of $Cd_xSr_{1-x}TiO_3$ with the $^{111}Cd(\leftarrow{}^{111m}Cd)$ probe, concentration dependence of occupation site of Cd was observed: Cd occupies random site up to an Cd ratio $0.005 \leqq x < 0.04$, and at Cd ratio x = 0.06, Cd dopants replace Sr^{2+} and Ti^{4+} in the lattice sites where defect exists in the vicinity of the probes. In order to obtain further information on concentration dependence of local structures at Cd sites in $Cd_xSr_{1-x}TiO_3$, we have thus performed TDPAC measurements for $Cd_xSr_{1-x}TiO_3$ with $^{111}Cd(\leftarrow{}^{111m}Cd)$ probe by doping wide concentration of Cd ions ($0.06 \leqq x \leqq 0.20$).

EXPERIMENTS: Stoichiometric amount of $SrCO_3$, $CdCO_3$, and TiO_2 powders were mixed in the mortar. The powders were pressed into disks. For TDPAC measurements, about 3 mg of CdO enriched with ^{110}Cd was irradiated with thermal neutrons in Kyoto University Research Reactor, and radioactive ^{111m}Cd was generated by $^{110}Cd(n, \gamma)^{111m}Cd$ reaction. The neutron-irradiated CdO powder was dissolved in 6M HCl and added in droplets onto the pre-sintered $Cd_xSr_{1-x}TiO_3$ disk. The disk was sintered in air at 1373 K for 90 min. The TDPAC measurement was carried out for the 151-245 keV cascade γ rays of $^{111}Cd(\leftarrow{}^{111m}Cd)$ probe with the intermediate state of $I = 5/2$ having a half-life of 85.0 ns.

RESULTS: Figure 1 shows the TDPAC spectra of $^{111}Cd(\leftarrow{}^{111m}Cd)$ (a) in $Cd_xSr_{1-x}TiO_3$ (x = 0.04), (b) in $Cd_xSr_{1-x}TiO_3$ (x = 0.06), and (c) in $Cd_xSr_{1-x}TiO_3$ (x = 0.20) at room temperature. The directional anisotropy on the ordinate, $A_{22}G_{22}(t)$, was deduced with the following simple operation for delayed coincidence events of the cascade:

$$A_{22}G_{22}(t) = \frac{2[N(\pi,t) - N(\pi/2,t)]}{N(\pi,t) + 2N(\pi/2,t)}. \qquad (1)$$

Here, A_{22} denotes the angular correlation coefficient, $G_{22}(t)$ the time-differential perturbation factor as a function of the time interval, t, between the relevant cascade γ-ray emissions, and $N(\theta,t)$ the number of the coincidence events observed at angle, θ. With respect to Fig. 1(a), the spectral pattern is damped. The spectral pattern was fit-ted with two static electric quadrupole frequencies which have large distribution widths (%)21(28 ,%)7(72 = δ). These large values of distribution widths indicate local randomness at $^{111}Cd(\leftarrow{}^{111m}Cd)$ probe sites in $Cd_xSr_{1-x}TiO_3$. As for the spectrum in Figs. 1(b) and 1(c), spectral patterns can be reproduced by a fit with unique quadrupole fre-quencies. It is suggested from our previous study that Cd dopants replace Sr^{2+} and Ti^{4+} in the lattice sites where de-fect exists in the vicinity of the Cd probes at Cd ratio x = 0.06 and x = 0.20. These results indicate that Cd ions dis-persed into $Cd_xSr_{1-x}TiO_3$ perovskite structure at high con-centration $0.06 \leqq x \leqq 0.20$. These concentration depend-ences of local structure at Cd site might be attributed to the change of lattice constant of $Cd_xSr_{1-x}TiO_3$. For more in-formation on these concentration dependence, investiga-tions of lattice constants of $Cd_xSr_{1-x}TiO_3$ perovskite are now in progress.

REFERENCE:

[1] C. M. Culbertson *et al.*, Scientific Reports, **10** (2020) 3729.

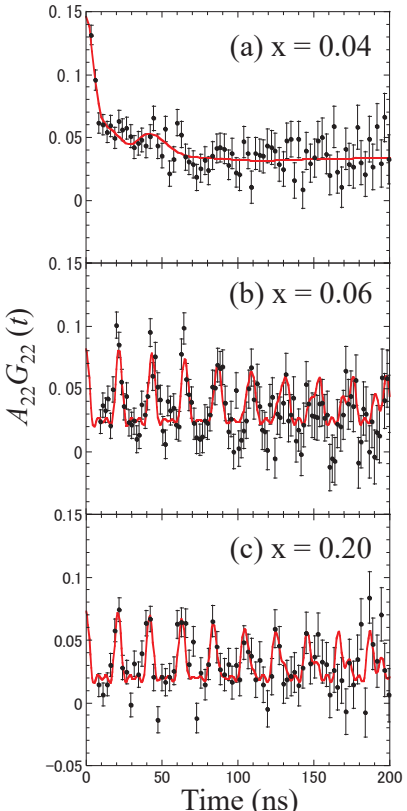

Fig. 1. TDPAC spectra of $^{111}Cd(\leftarrow{}^{111m}Cd)$ (a) in $Cd_xSr_{1-x}TiO_3$ (x = 0.04), (b) in $Cd_xSr_{1-x}TiO_3$ (x = 0.06) and (c) $Cd_xSr_{1-x}TiO_3$ (x = 0.20) at room temperature.

CO4-7 Hydrogen trapping behavior at vacancy in Fe-Al alloy with electron irradiation

F. Hori, S. Hirayama, H. Obayashi, J. Tian, K. Ohsawa[1], Q. Xu[2], N. Abe[2] and K. Yasunaga[3]

Osaka Metropolitan University
[1]*Res. Inst. of Appl. Mech., Kyushu University*
[2]*Institute for Integrated Radiation and Nuclear Science, Kyoto University*
[3]*Wakasa-wan Energy Research Center*

INTRODUCTION: Intermetallic compound of Fe-Al alloy is used as high strength at high temperature material because of its good properties such as specific strength to weight ratio, oxidation resistance. However, it is known that Fe-Al alloy with B2 ordered structure is easy to form vacancy and anti-site atom defects. These defects strongly affect the physical and mechanical properties. We have investigated the nature of defect structures in B2 type Fe-Al alloy [1,2]. On the other hand, the vacancy type defects in this alloy first principles calculation result indicate that not only one hydrogen atom but also several hydrogen atoms can be trapped in a single vacancy in B2 ordered Fe-Al alloy. However, the interaction between vacancies and hydrogen atoms in this type of Fe-Al alloy is not cleared yet. Our previous works have shown that hydrogen atoms are trapped in the introduced vacancies introduced by electron irradiation. We have also reported that hydrogen atoms trapped in the vacancies are released by annealing above 500 K [3].

EXPERIMENTS: B2 ordered Fe-Al alloys were prepared by arc melting method in argon gas atmosphere. Sliced samples with the thickness of 0.5 mm were annealed at 1273 K for 20 h and cool down to 973 K slowly and then quenched into water. These specimens were irradiated with 8 MeV electron up to the fluence of 4×10^{18} /cm^2 at KURRI, Kyoto University. Irradiation was carried out at about 330 K with temperature controlling water cool system. Hydrogen was injected for electron irradiated samples at 0.1 mA/cm^2 in a NH_4SCN solution bath added 0.001 mol/L H_2SO_4 by electro chemical method for 8, 16, 80 and 160 hours. These samples were examined by positron annihilation coincidence Doppler broadening measurement. Also, the thermal desorption spectroscopy (TDS) was measured with heating rate of 1 K/s.

RESULTS: Figure 1 shows the CDB ratio curves of H-injected Fe-Al alloy normalized to that of the alloy before hydrogen injection. The ratio curve changes with H-injection and decreases around 0 m_0c suggesting that hydrogen atoms are trapped in the vacancies. Fig. 2 shows the TDS spectra for hydrogen injected Fe-Al alloys after 8 MeV electron irradiation. This figure clearly shows that the amount of absorbed hydrogen becomes larger with hydrogen charging time. In addition, absorption peak appears around 650 K shifted to lower temperature with increasing hydrogen charging time. This may be due to the change in the ratio of vacancies to hydrogen atoms, which may result in a change in the state of hydrogen trapping. This result also suggests that multiple hydrogen may be trapped in a single vacancy.

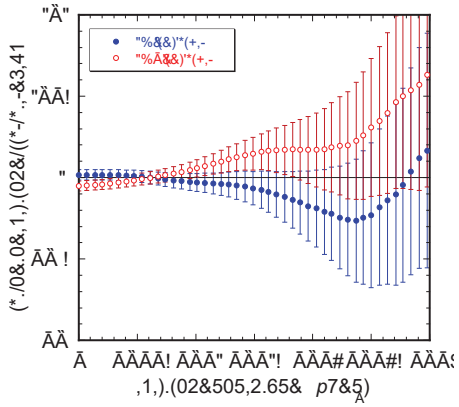

Fig. 1. CDB ratio spectra of 16 and 160 hr hydrogen injected Fe-Al alloy after electron irradiation.

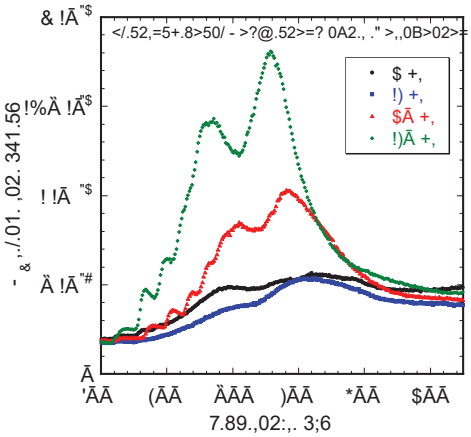

Fig. 2. TDS spectra of Fe-Al alloy electrochemicaly implanted with hydrogen after electron irradiation.

REFERENCE:

[1] T. Haraguchi, *et al.,* Intermetallics, **9** (2001) 763-770.
[2] F. Hori *et al.,* JJAP Conf. Proc., **9** (2023) 011107.
[3] F. Hori *et al.,* KURRI Progress Report 2021, (2022)114.

CO4-8 Metal nano-composites formation in water solution by electron irradiation reduction

F. Hori, S. Matsuo, T. Matsui[1], N. Taguchi[2], S. Tanaka[2], H. Tanimoto[3] and Q. Xu[4]

[1]*Osaka Metropolitan University*
[2]*AIST, Kansai Center*
[3]*University of Tsukuba*
[4]*Institute for Integrated Radiation and Nuclear Science, Kytoto University*

INTRODUCTION: Metal nanoparticles (NPs) have some specific properties, which are not appeared in bulk materials such as catalytic activities, magnetic properties, electric conductivity and light absorption. They have many possibilities to applied for various industrial fields. However, it is not easy to fabricate multi elemental alloy NPs with controlling their size, shape and structure. Generally, many kinds of metal NPs commercially are synthesized by using chemical reaction method, which is not necessarily in water solution. Recently, it is possible to fabricate some metal NPs under irradiation reduction fields such as ultrasonic, solution plasma, electron beam, ion beam and gamma-ray [1]. On the other hand, metal nanoparticles with high electronic conductivity are expected for the fields of printed electronics technologies as a metal nano-ink. Cu is the high electronic conductivity and one of the most abundant resources on earth. However, the fabrication of Cu nanoparticle has a difficulty because its oxidation property. So far, we have successfully synthesized pure Cu nanoparticles by gamma-ray reduction method. In this study, we have tried to synthesize Ag-Cu-X (X=Au, Ni) nano size composite particles by electron irradiation reduction.

EXPERIMENTS:

Aqueous solution with a 0.5 mM copper complex ($(CH_3COO)_2Cu{\cdot}H_2O$), 0.5 mM gold complex ($NaAuCl_4{\cdot}2H_2O$) with an additive of sodium dodecyl sulfate (SDS) and 8.5 vol% ethylene glycol was prepared. 0.5 mM $AgNO_3$ and 0.5 mM $NiCl_2$ was added into each solution, separately. The solutions were argon gas purged and sealed into polystyrene vessels. They were irradiated 7.5 MeV electron with total dose of 15 kGy in about 52 sec by linear accelerator at KURRI Kyoto University. After irradiation, the samples were measured for UV–vis absorption, X-ray Photoelectron Spectroscopy (XPS) and X-ray absorption fine structure (XAFS) at KEK BL-27 and small angle X-ray scattering (SAXS) at KEK BL-6. Moreover, dried and filtered samples were measured by X-ray diffraction and TEM (JEM-2000FX and FEI-Titan).

RESULTS:

In each sample, color of solution was clearly changed by electron irradiation, suggesting that the solute ions were reduced and formed nanoparticles. Fig. 1 shows the XRD profiles of AgCuNi and AgAuCu samples. In both cases, clear CuO (110) bragg peak and some peaks of fcc Ag are observed. On the other hand, the results of XAFS and XPS show that Cu-Cu and Cu-Ni atomic bonds were confirmed. Fig. 2 shows the SAXS profiles of the AgCuNi and AgAuCu solutions after electron irradiation and the reduced sample after gamma-ray irradiation as a comparison. This figure shows that the size of the formd particles in the case of AgCuNi are similar between electron and gamma-ray irradiation, while the size and other state of the formed particles in the case of AgAuCu are different. These results indicate that when the three types of ions are reduced simultaneously by electron irradiation, oxides are formed, but Cu and Ni are also reduced based on Ag, and complexes containing small amounts of other ions are formed.

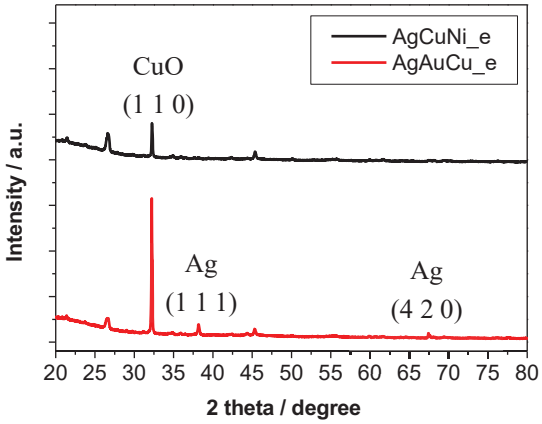

Fig.1. XRD profiles of electron irradiated AgCuNi and AgAuCu samples.

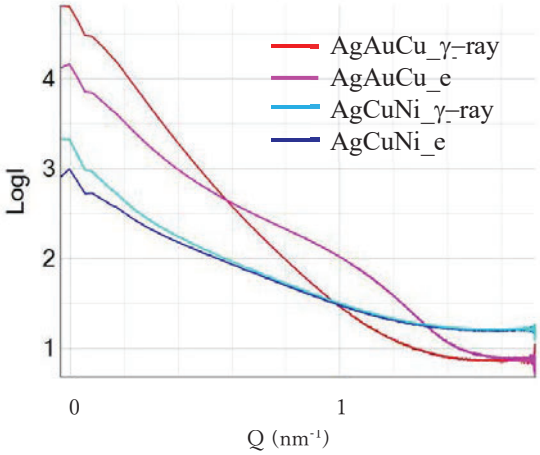

Fig. 2. SAXS spectra of AgAuCu and AgCuNi solutions after electron and gamma-ray irradiation.

REFERENCES:

[1] N. Taguchi *et al.,* Rad. Phys. Chem., **78** (2009) 1049-1053.

CO4-9 Slow Positron Beam Analysis of Polymer Composite Materials

Z. Chen, Y. Kobayashi[1], A. Yabuuchi[2] and A. Kinomura[2]

Department of Material Science and Engineering, Wuhan Institute of Technology, People's Republic of China

[1]Waseda Research Institute for Science and Engineering, Waseda University

[2]Institute for Integrated Radiation and Nuclear Science, Kyoto University

INTRODUCTION: 2D membranes based on the 2D materials, such as graphene oxide (GO) and $Ti_3C_2T_x$ (MXene), can be applied for molecular sieving with high flux and energy efficiency. It was believed that the interlayer spacing between the nanosheets was one of the key factors those influence the molecular sieving effect. So far, the popular method to evaluate the interlayer spacing is XRD. And the interlayer distance can be calculated using Bragg's law. However, this distance includes the thickness of the nanosheet and the electronic clouds of the polar groups grafted on the nanosheet. In fact, the channel for the molecules permeating through the 2D membrane is an 'empty' space in the interlayer spacing. To achieve the selective rejection of the 2D membranes, different groups were grafted on the nanosheets. In this case, the XRD results may not be so precise to predict membrane performance. It is necessary to develop new method to measure the voids between the nanosheets which are in charge of the ion permeation.

In this study, positron beam was utilized to evaluate the voids between the nanosheets. Doppler broadening spectroscopy coupled with positron beam was used to analyze the layer structure of the 2D membranes, while the positron lifetime measurement coupled with positron beam was applied to probe the voids between the 2D nanosheets.

EXPERIMENTS: GO/MXene/substrate and MXene/GO/substrate membranes were prepared by vacuum filtration method. First, 20-ml GO/water solution with a concentration of 0.005 mg/ml was filtrated by polyether sulfone (PES) substrate at 0.1 MPa. And then the 20-ml MXene/water solution with a concentration of 0.005 mg/ml was filtrated by GO/substrate membrane. And the obtained sample was MXene/GO/substrate. The GO/MXene/substrate membrane was obtained with the similar method. The as prepared membranes were heated in oven for 4 hours at 170 °C, and labeled as heated ones. Positron annihilation Doppler broadening and lifetime measurements were performed with the positron beam system at the Institute for Integrated Radiation and Nuclear Science, Kyoto University.

RESULTS: As shown in Fig. 1, the layer structure of the four samples can be distinguished from *S*-*E* curves. It can be seen that, the *S*-*E* curves can be divided into three stages, surface layer (0~5 keV), beneath layer (5~12 keV) and substrate. It is seen that the heat treatment of the beneath layer results in lower *S* parameters. Moreover, the positron lifetime results at an incident energy of 8 keV in Table 1 show that the long-lived *ortho*-positronium (*o*-Ps) component is present in the as prepared samples but not in the heated ones. It can be concluded that the heat treatment led to the inhibition of the formation of positronium (Ps).

Traditionally the size of the void for molecule permeation through the 2D membrane was calculated by coupling the results from XRD and AFM [1]. The interlayer spacing distance can be determined by XRD, and the thickness of a single platelet can be probed by AFM. Considering that the electronic clouds around graphene sheets extend over a distance of ~ 3.34 Å, the 'empty' space available for gas molecules to diffuse is estimated around 5 Å for the GO membranes by Ibrahim and Lin [2]. The positron beam experiment has the potential for independent estimation of this 'empty' space. We further seek this possibility in this ongoing research.

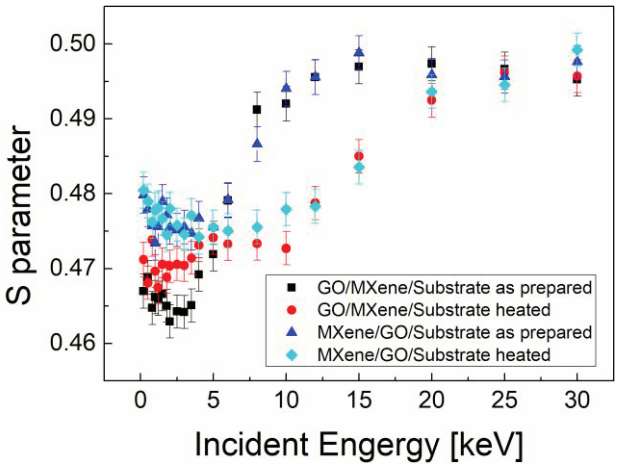

Fig.1. The *S*-*E* plots for the samples.

Table 1. *o*-Ps lifetime results at 8 keV.

	o-Ps lifetime (ns)	*o*-Ps intensity (%)
GO/MXene/Sub	1.54±0.03	14.8±0.4
GO/MXene/Sub heated	-	-
MXene/GO/Sub	1.62±0.03	13.8±0.3
MXene/GO/Sub heated	-	-

REFERENCES:

[1] R.R. Nair *et al.*, Science, **335** (2012) 442-444.

[2] A. Ibrahim and Y. S. Lin, J. Membrane Sci., **550** (2018) 238-245.

CO4-10 Characterization of Precipitates in Cu alloy using Small-Angle X-ray Scattering

Y. Oba and H. Sasaki[1]

Materials Sciences Research Center, Japan Atomic Energy Agency
[1]Furukawa Electric Co., Ltd.

INTRODUCTION: Cu alloys are one of the most important materials supporting a wide variety of industries with excellent electric and mechanical properties. In the Cu alloys, precipitation strengthening is effective to further improve the strength with reasonable conductivity [1,2]. In the precipitation-strengthened Cu alloys, the size and morphology of the precipitates are directly connected to the strength, while the alloying elements dissolved in matrix decreases the conductivity. Therefore, quantitative characterization of the precipitates is required to optimize the precipitation conditions. Small-angle X-ray scattering (SAXS) is a powerful means for such quantitative characterization of the nanostructures in metals and alloys [3,4]. In this study, we performed the SAXS measurement of Cu-Ni-Si, which is a typical precipitation-strengthened Cu alloy.

EXPERIMENTS: The chemical composition of the samples was Cu-2.5mass%Ni-0.6mass%Si. The ingot was solution-treated and aged for two hours at various temperatures. SAXS measurements were performed using the SAXS instrument with Mo *K*α radiation. Scattering patterns were measured using a photon-counting-type two-dimensional detector (PILATUS 100k). The converter was a silicon with the thickness of 1000 μm to detect the high energy X-ray from Mo efficiently. The X-ray path between an entrance slit and a detector window was in vacuum to reduce background scattering from air. The data reduction was conducted using our original program written in Igor Pro software.

RESULTS: In two-dimensional scattering patterns, all the samples show isotropic scattering. This means that the precipitates are isotropically dispersed in the samples (Fig. 1). Fig. 2 shows the circularly averaged scattering profiles. All the samples have higher intensities than the background. For the as-solution-treated sample, the scattering profile decreases exponentially with increasing q and then exhibits a plateau at $q > 3$ nm^{-1}, where q denotes the magnitude of the scattering vector. This q dependence is a typical background contribution from solution-treated alloys [4], where no precipitates are dispersed ideally. Compared to the as-solution-treaded sample, the other profiles have a shoulder, which indicates the formation of the precipitates. With increasing aging temperature, the shoulder shifts toward lower q. This means that the precipitates become larger. As a result, we successfully ob-served the formation of the precipitates and their growth with aging temperature in Cu-Ni-Si using SAXS. These results agree well with the tendency obtained using small-angle neutron scattering (SANS) [5].

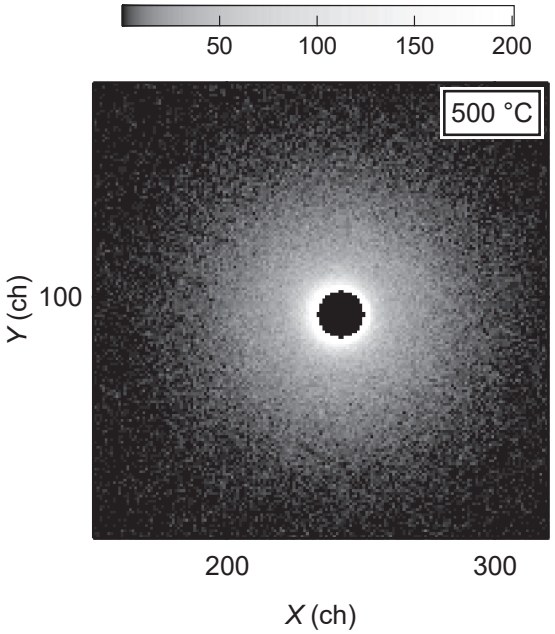

Fig. 1. Typical two-dimensional scattering pattern of Cu-Ni-Si aged at 500 °C.

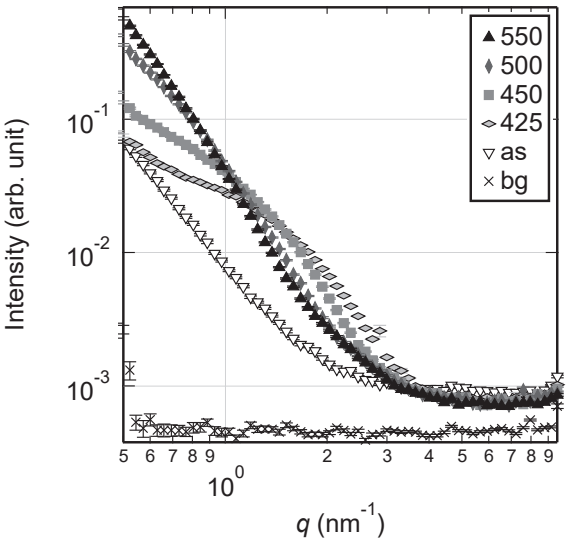

Fig. 2. Scattering intensity of Cu-Ni-Si aged at 425, 450, 500, and 550 °C as well as solution-treated.

We are now characterizing the detail of the internal structure of the precipitates from the comparison of SAXS and SANS [5].

REFERENCES:

[1] S. A. Lockyer *et al.*, J. Mater. Sci., **29** (1994) 218-226.
[2] H. Fujiwara *et al.*, J. Jpn. Inst. Metals, **62** (1998) 301-309.
[3] M. Ohnuma *et al.*, Acta Mater., **57** (2009) 5571-5581.
[4] Y. Oba *et al.*, ISIJ Int., **55** (2015) 2618-2623.
[5] H. Sasaki *et al.*, Mater. Trans., **63** (2022) 1384-1389.

CO4-11 Gamma-ray induced photo emission from GaP single crystal wafer: Comparison with GaN

T. Nakamura[1], T. Nishimura[1], K. Kuriyama[1], Atsushi Kinomura[2]
[1]*Research Center of Ion Beam Technology, Hosei University, Koganei, Tokyo 184-8584, Japan*
[2]*Institute for Integrated Radiation and Nuclear Science, Kyoto University, Kumatori, Osaka 590-0494, Japan*

INTRODUCTION: Gallium phosphide (GaP) is usually employed in the manufacture of low-cost red, orange, and green light-emitting diodes (LEDs). We recently succeeded in detection of the gamma-ray induced photo emission from GaN [1] and ZnO [2] single crystal wafers. Whether the luminescence by the excitation of gamma-ray is observed at room temperature in GaP as similar to GaN and ZnO is important as it may be used as an application as a gamma-ray detector. In the present study, we investigate the luminescence properties in gamma-ray excition of GaP, and the difference in gamma-ray induced photo emission from GaN, which is transparent to visible light.

EXPERIMENTS: GaP single crystal wafers with a size of several cm square and a thickness of several 100 μm meters were used for the present study. The crystals were irradiated at room temperature with gam-ma-rays of 1.17 and 1.33 MeV from a cobalt-60 source of Institute for Integrated Radiation and Nuclear Science, Kyoto University. The gamma-ray irradiation induced photo emission measurements were performed by using a charge coupled device (CCD) equipped spectrometer (QE Pro, Ocean Insight Co. Ltd.). Each measurement was performed under 20 min, gamma-ray irradiation and each spectrum was acquired for 2 min, CCD exposure time. One end of a 10-meter long optic fiber cable made of SiO_2 was set on the front face of GaP placed near the Co source and the other end was led to the analysis room with the spectrometer. The transmission of this fiber is about 90 % at wavelengths from 475 to 1300 nm and about 50 to 85 % at wavelength from 380 to 475 nm. Therefore, gamma-ray induced photo emission measured using this fiber cable may reduce the band edge emission of wide gap semiconductors such as GaN.

RESULTS: Figure 1 shows Gamma-ray induced photo emission spectra of GaP and GaN single crystal wafers. Both spectra are broad. The greater breadth of the spectra observed in GaP can be attributed to donor-acceptor pair transitions [3]. These spectra are usually broad because of strong phonon-assisted transitions arising from the tight binding of the O donor.Emission intensity of GaP is lower than that of GaP wafer. This lower emission intensity is observed in normal photoluminescence measurement using a He-Cd laser. The peak intensity from impurity doped GaP is about 1/200 of GaN. The transparent GaN has a larger penetration depth for the He-Cd laser and a higher emission intensity. On the other hand, it is suggested that GaP is opaque, has less penetration of He-Cd laser light than GaN, and also shows the low emission intensity. More importantly, un-doped GaP show no photoluminescence. In GaN with native defects, the defect level behaves as the emission center without adding impurities. Yellow luminescence (YL) observed in GaN has been proposed as a transition from a shallow donor to gallium vacancy (VGa) located at about 1.1 eV above the valence band [4]. Our previous study [5] reported that the high-dose gamma-ray irradiation of 160 kGy mainly induces N vacancies (VN) located at about 50 meV below the conduction band. Therefore, the gamma-ray induced YL observed in GaN is attributed to a shallow donor to VGa transition due to the excitation from valence band to conduction band by Compton electrons.

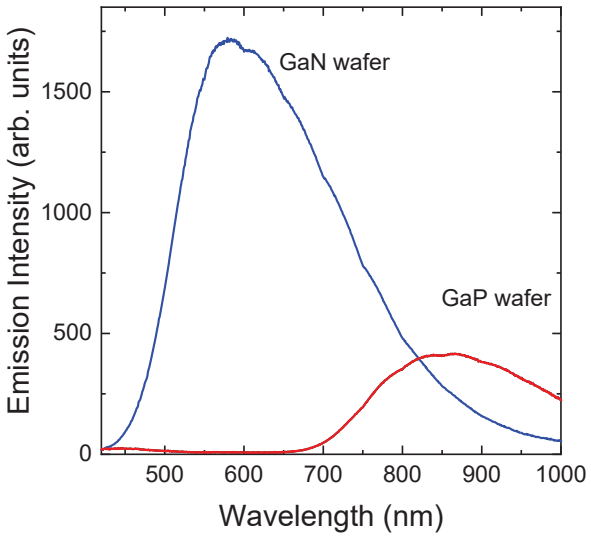

Fig. 1. Gamma-ray induced photo emission spectra from GaN and GaP single crystal wafer.

Part of this research was submitted to Nuclear Instruments and Methods in Physics Research Section B: Beam Interactions with Materials and Atoms.

REFERENCES:

[1] T. Nakamura *et al.*, Appl. Phys. Lett., **118** (2021) 032106.
[2] T. Nakamura *et al.*, Solid State Commun., **336** (2021) 114413.
[3] P. J. Dean *et al.*, Phys. Rev., **168** (1968) 812.
[4] J. Neugebauer *et al.*, Appl. Phys. Lett., **69** (1996) 503.
[5] Y. Torita *et al.*, J. Phys.: Conf. Series, **864** (2016) 012016.

CO4-12 Porosity control of diamond-like carbon films

S. Nakao, X. Qu[1], A. Yabuuchi[1] and A. Kinomura[1]

Innovative Functional Materials Research Institute, National Institute of Advanced Industrial Science and Technology
[1]Institute for Integrated Radiation and Nuclear Science, Kyoto University

INTRODUCTION: Diamond-like carbon (DLC) films which sometimes include hydrogen have attracted much attention because of their excellent properties. However, their properties are strongly degraded at elevated temperature. It is considered that the degradation should be related to the release of hydrogen and the structural changes at feverish temperature. Moreover, the behavior of pores which are presented due to amorphous nature also may be significant role on the degradation. Regrettably, the behavior of the pores in the films is not always clarified up to now.
Positron annihilation spectroscopy (PAS) using energy-variable monoenergetic positron beams (slow positron beams) is a useful technique which enables to investigate the behavior of pores in amorphous thin films. It is known that S parameters obtained from Doppler broadening annihilation radiation (DBAR) measurement reflect the size and density of open-volume defects or pores with the information of annihilation sites in the films. On the other hand, positron lifetime obtained by positron annihilation lifetime spectroscopy (PALS) mainly reflect the size of open volume defects or pores. Therefore, it is expected that both DBAR and PALS measurements should be useful for the examination of the behavior of pores as a function of annealing temperature.
In this study, DLC films are prepared by a bipolar-type plasma-based ion implantation and deposition (PBIID) system. The samples are annealed in vacuum in the range of 200 – 800 ºC. The behavior of pores is examined by PAS measurement.

EXPERIMENTS: The bipolar-type PBIID system [1] was used for sample preparation. Toluene (C_7H_8) or acetylene (C_2H_2) was used as source gas for the deposition of DLC films which were denoted as sample A and sample B, respectively. Silicon (100) wafers were used as substrates which were cut into 2 x 2 cm. The substrates were put on the sample holder where positive pulse voltage was applied, and then negative pulse voltage was applied at a frequency of 2 kHz. The deposition time of sample A and B were 40 and 60 min, respectively.
The samples were annealed in vacuum by infrared image furnace. The furnace was evacuated less than 3 x 10^{-3} Pa by a turbo molecular pump. The heating rate was 100 ºC/min and the annealing time was 60 min. The annealing temperature was set ranging from 200 to 800 ºC. The samples were kept in vacuum after annealing process and naturally cooled down to room temperature. PAS measurement was performed with a slow positron beam line. S parameters as function of energy (S-E curves) were measured in the range of 0 – 26 keV. Lifetime measurement was also conducted with a positron beam at an energy of 2 keV.

RESULTS: To investigate the pores in DLC films, the relationship between the S parameter and lifetime is plotted in Fig. 1. For sample A, the S parameter only decrease up to 400 ºC. This result seems that the pores decrease in number. However, it is noted that S parameter may be insensitive to the number of pores due to the saturation effect. Therefore, it is considered that the decrease of S parameter should be caused by the increase of π electron in number. At 800 ºC, the lifetime increases accompanied with decreasing S parameter. This suggests that the pores increase in size and π electrons increase in number. For the sample B, the S parameter mainly increases up to 400 ºC, suggesting that the pores mainly increase in size. At the same time, π electrons possibly increase in number, which is competitive effect to S parameter. At further increase of annealing temperature, the trend is a little bit complicated. At 600 ºC, the lifetime and S parameter increase. However, both values are rapidly decrease at 800 ºC. From the results, it is suggested that the pores once increase in size at 600 ºC. And then the pores decrease in size and π electrons possibly increase in number at 800 ºC.

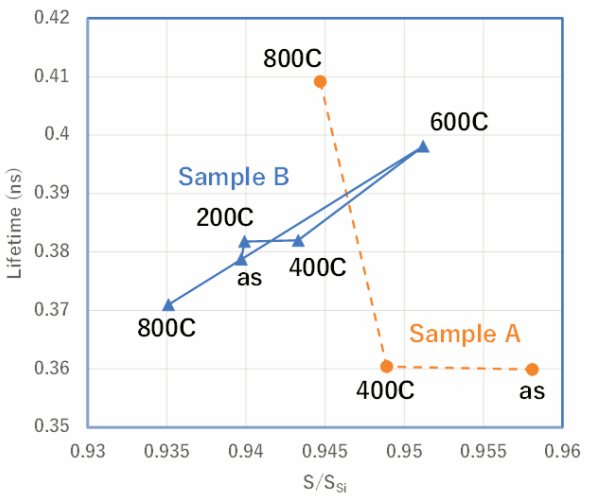

Fig.1. Relationship between the S-parameters and the lifetimes for respective samples A and B.

REFERENCES:
[1] S. Miyagawa *et al.*, Surf. Coat. Technol., **156** (2002) 322-327.

CO4-13 Hyperfine Fields in $La_{0.7}Ca_{0.3}Mn_{0.45}Fe_{0.55}O_3$ Measured by Means of Mössbauer and TDPAC Spectroscopies

W. Sato, H. Uchino[1], K. Takanashi[2], S. Komatsuda[3], A. Taniguchi[4], M. Tanigaki[4], and Y. Ohkubo[4]

Institute of Science and Engineering, Kanazawa University
[1]Graduate School of Science and Technology, Kanazawa University
[2]School of Chemistry, Kanazawa University
[3]Institute of Human and Social Sciences, Kanazawa University
[4]Institute for Integrated Radiation and Nuclear Science, Kyoto University

INTRODUCTION: $La_{0.7}Ca_{0.3}MnO_3$ is a metal oxide with a perovskite structure in which La and Ca occupy the *A* site and Mn the *B* site, respectively [1]. This compound has been receiving high expectations for applications to spintronics devices because of the effect of colossal magnetoresistance below $T_C \sim 250$ K arising from double exchange interaction caused by the electron transfer between Mn^{3+} and Mn^{4+} [2]. The CMR effect is expected to be applied to a variety of functional materials such as magnetic heads and resistance change memories. For wide applications of this compound, it is preferable to control its magnetic property for each practical use. As the first trial to control its magnetic property, in the present study, we tried to raise the transition temperature T_C to the vicinity of room temperature by introducing Fe to the *B* site substituting for Mn by 55% to synthesize $La_{0.7}Ca_{0.3}Mn_{0.45}Fe_{0.55}O_3$ (LCMFO). For the measurements of the local magnetic fields, we employed ^{57}Fe transmission Mössbauer and TDPAC spectroscopies. Here, a preliminary result is reported.

EXPERIMENTS: Stoichiometric amounts of La_2O_3, MnO_2, Fe_2O_3, and $CaCO_3$ were mixed well in a mortar, and the powdery mixture was calcined at 1273 K for 12 h. The sample was again ground to uniformity and was pressed into a disk. The disk was then sintered at 1473 K for 96 h. Successful synthesis of LCMFO was confirmed by the powder X-ray diffraction pattern.
A ^{57}Fe Mössbauer spectrum was obtained for the sample at room temperature (RT). The velocity of the source was calibrated with α-Fe at RT.
Neutron irradiation was performed for cadmium oxide (CdO) enriched with ^{110}Cd in Kyoto University Reactor to produce radioactive ^{111m}Cd. The radioactive Cd(^{111m}Cd)O powder was mixed well with the powdery LCMFO sample. The mixture was then pressed into a disk and was sintered in air at 1373 K for 45 min. A TDPAC measurement was carried out for the ^{111}Cd(←^{111m}Cd) probe with the intermediate state of I = 5/2 having a half-life of 85.0 ns. In the present work, we obtained the spectrum with four detector system to observe delayed coincidence events at 90 and 180 degrees' angular correlation of the 151-245 keV cascade γ rays.

RESULTS: The RT ^{57}Fe Mössbauer spectrum obtained for $La_{0.7}Ca_{0.3}Mn_{0.45}Fe_{0.55}O_3$ is shown in Fig. 1(a). The spectrum is dominated by an intense doublet, suggesting that most of the ^{57}Fe spins are paramagnetically fluctuated at this temperature. However, a quite broad resonant component is also observed in the spectrum, possibly indicating a transitional shift of the spin state between paramagnetic and ferromagnetic ordering. This observation may suggest that T_C has successfully been raised to RT or higher. For more information, we obtained a TDPAC spectrum of the ^{111}Cd(←^{111m}Cd) probe at RT as shown in Fig. 1(b). The spectrum shows a wide distribution of the electric quadrupole frequency for the precession of the probe. Although the fit was based on the assumption that the probes are perturbed by the electric quadrupole interaction with the outer charge distribution, the wide distribution could be attributed to slow fluctuation of the spins of the magnetic Mn and Fe ions at the *B* site. For more detailed discussion, low temperature measurements are underway.

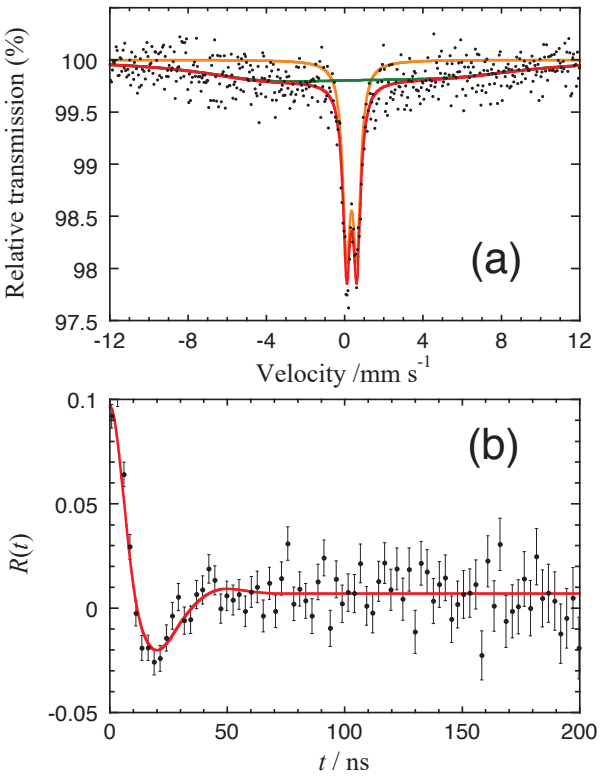

Fig. 1. (a) ^{57}Fe Mossbauer spectrum and (b) TDPAC spectrum of ^{111}Cd(←^{111m}Cd) obtained for $La_{0.7}Ca_{0.3}Mn_{0.45}Fe_{0.55}O_3$ at room temperature.

REFERENCES:

[1] H. Y. Huang *et al.,* Phys. Rev. Lett., **75** (1995) 914-917.
[2] W. Sato *et al.,* Phys. Rev. B, **100** (2019) 184111/1-7.

CO4-14 A study of guar-gum hydrogels using small angle X-ray scattering

T. Tominaga[1], R. Inoue[2], and M. Sugiyama[2]

[1]*Neutron Science and Technology Center, Comprehensive Research Organization for Science and Society (CROSS)*
[2]*Institute for Integrated Radiation and Nuclear Science, Kyoto University*

INTRODUCTION: One of the characteristics of soft matter is its capability of large deformation. Polyvinyl alcohol-borate hydrogel (so-called slime), consisting of polyvinyl alcohol (PVA), borax, and water, has long been known as a toy, and is a soft matter known to be capable of large deformation. Additives to hydrogels inhibit/promote the mechanical properties of the hydrogel.

Cross-linking agents, which are used to retain the gel morphology to some extent, lead the hydrogel less deformable, depending on the additive amount. Lubricants that act between polymer chains also be introduced to make polymer chains smoother and facilitate large deformations.

Hydrogels prepared with guar gum (GG), a galactomannan, can be greatly deformed by the addition of appropriate amounts of borax (cross-linking agent), glycerin, and vinyl acetate resin particles, compared to GG gel, which has only borax as an additive.

In this experiment, for hydrogels created with GG, the internal structural changes of the hydrogels due to the addition of borax (cross-linking agent), lubricants, and particles were evaluated by small-angle X-ray scattering (SAXS).

EXPERIMENTS: GG hydrogels were prepared in the following weight ratios: GG: approximately 2–3 wt.%, glycerin 7 ml, borax: approximately 0.4 g, vinyl acetate granular resin: approximately 2–3 g, and water: approximately 88 g.

The sample thickness of hydrogels was approximately 0.5 mm and sandwiched between a polyetherimide resin (Sperio, Mitsubishi, Japan). The Cu-SAXS (RIGAKU Nanopix) available at Institute for Integrated Radiation and Nuclear Science, Kyoto University of high-resolution mode was utilized. The empty cell was subtracted to account for the transmission, and the scattering profile, $I(Q)$ was obtained by circular averaging.

RESULTS: SAXS profiles of GG hydrogels are shown in Fig. 1. The simple GG (+ water) scattering profile shows that the addition of borax increases the slope and the addition of glycerol decreases the slope; the addition of resin increases the slope at $Q < 0.2$ Å^{-1}.

Considering that the change in slope is correlated with the internal structural inhomogeneity of the substance, glycerol has a structural homogeneity effect on slime, borax has a structural imhomogeneity effect, and resin has a structural inhomogeneity effect at $Q < 0.2$ Å^{-1}. Although the size of the resin is in the order of micrometers, the effect of the resin on the polymer chains could be observed in this SAXS Q range.

PVA is known to easily form nanocrystals with a size of approximately 7 nm [1]. The effects of the introduction of additives on hydrogel structure were evaluated in the same way as for GG hydrogels. The effects of each additive on the structure of PVA were similar to those of GG, however the effects were not strong enough to block the formation of nanocrystals. In the case of GG hydrogels, no internal structure corresponding to microcrystals was observed in the scattering profiles of PVA hydrogels, suggesting that the ability to form microcrystalline structures is an obstacle to large deformation.

Data were also obtained on the structure of the hydrogel in the case of other galactomannan species, the effect of lubricants other than glycerol, and the size-dependence of glass particles as a substitute for the resin. The data will be individually investigated and compiled into an original paper.

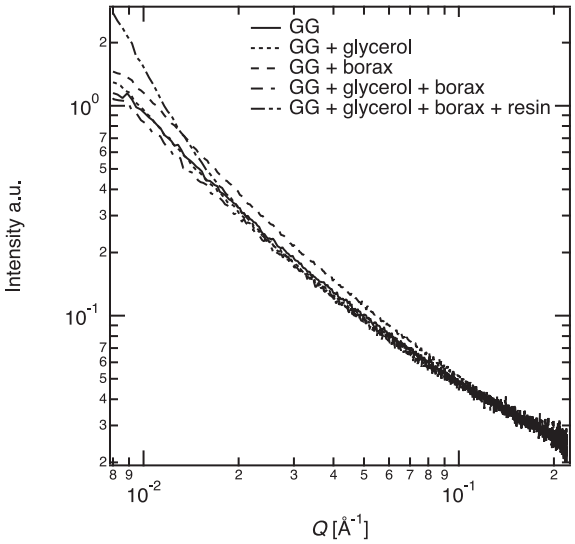

Fig. 1. SAXS profile of GG + water with additives (glycerol, borax, and vinyl acetate granular resin). Each profile corresponds to the presence or absence of the additives.

REFERENCES:

[1] T. Kanaya *et al.,* Polymer Journal, **44** (2012) 83-94.

CO4-15 Tritium recovery behavior for tritium breeder Li_2TiO_3-Li_4SiO_4 biphasic materials with various phase ratios and Pb addition

Y. Oya[1], A. Sanfukuji[2], Q. Zhou[3], G. Tan[4], F. Sun[5], Y. Feng[6], X. Wang[6], H. Wang[7], M. Kobayashi[8], Y. Iinuma[9] and R. Okumura[9]

1 Faculty of Science, Shizuoka University
2 Graduate School of Integrated Science and Technology, Shizuoka University
3 School of Materials and Science Engineering, Wuhan University of Technology
4 School of Materials and Science Engineering, University of Science and Technology Beijing.
5 School of Material Science and Engineering, Hefei University of Technology
6 Fusion Technology Research Division, Center for Fusion Science, Southwestern Institute of Physics
7 College of Physics, Sichuan University
8 National Institute for Fusion Science
9 Institute for Integrated Radiation and Nuclear Science, Kyoto University

INTRODUCTION:

In the fusion reactor blanket, tritium is produced by (n, α) reaction with lithium. Lithium titanate (Li_2TiO_3) and lithium orthosilicate (Li_4SiO_4) are considered as candidates for solid tritium breeding materials. Li_2TiO_3-Li_4SiO_4 mixed ceramic materials are expected to have both advantages. Lead (Pb) is a neutron multiplier that contributes to the improvement of the tritium breeding ratio and tritium recovery efficiency due to lower affinity with tritium. However, the tritium recovery performance has not been evaluated. In this work, the effect of Pb addition on tritium recovery for Li_2TiO_3-Li_4SiO_4 mixed ceramic materials was investigated. Li_2TiO_3-Li_4SiO_4 biphasic materials with various phase ratios and Pb addition were used and their tritium desorption behaviors after neutron irradiation were evaluated by tritium thermal desorption spectroscopy (tritium-TDS).

EXPERIMENTS:

Three kinds of powder samples were used, including Li_2TiO_3-Li_4SiO_4 (LTO-LSO), Li_2TiO_3-0.5Li_4SiO_4 (LTO-0.5LSO), and Li_2TiO_3-Li_4SiO_4-5wt%Pb (LTO-LSO-5wt%Pb). Those samples were irradiated by neutron at Kyoto University Research Reactor (KUR) with the neutron fluence of 3.96×10^{16} n cm^{-2}. After the neutron irradiation, tritium release behavior was evaluated by tritium-TDS by heating the samples separately from R.T. to 1113 K with the heating rates of 10, 20, and 30 K min^{-1}. Liquid scintillation counter (LSC) was used to measure the total T amount trapped by the water bubbler at Shizuoka University.

RESULTS:

Fig. 1. shows the tritium-TDS spectra. By the comparison of T desorption behavior for LTO-LSO and LTO-0.5LSO, the T desorption peak has shifted toward lower temperature side as the percentage of LTO increased. With the addition of 5 wt% Pb, additional peak shift toward lower temperature side was confirmed, indicating that the addition of lead enabled tritium recovery at lower temperatures. Besides, almost all of tritium was released in the form of tritiated water (HTO), which was also confirmed by the LSC measurement, while gas-species (HT) release was observed for the LTO-LSO-5wt%Pb. This may be due to the fact that Pb, a neutron multiplier, has a low affinity for tritium. The activation energies of tritium desorption for each sample was calculated based on the kinetics analysis by heating the sample with various heating rates. The activation energies were 1.13 eV for LTO-0.5LSO, 0.76 eV for LTO-LSO, and 0.86 eV for LTO-LSO 5wt% Pb, respectively. The LTO-LSO sample has acheived the lowest value. It can be said that higher Li atomic density may facilitate stable trapping sites in LTO-LSO. In our future work, Pb concentration dependence on T release will be scheduled.

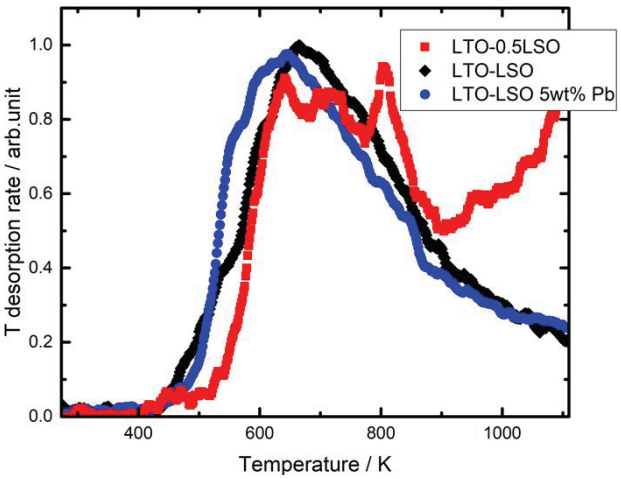

Fig. 1. Tritium-TDS spectra for Li_2TiO_3-Li_4SiO_4, Li_2TiO_3-0.5Li_4SiO_4 and Li_2TiO_3-Li_4TiO_4 5wt% Pb with the heating rate of 10 K min^{-1}.

REFERENCES:

[1] Q. Wang *et al.*, Ceramics International, **48** (2022) 26742-26749.

R4096

CO4-16 Study to improve transport and measurement performance of a slow positron beamline

A. Kinomura, N. Oshima[1], A. Uedono[2] and A. Yabuuchi

Institute for Integrated Radiation and Nuclear Science, Kyoto University
[1]National Institute of Advanced Industrial Science and Technology (AIST)
[2]University of Tsukuba

INTRODUCTION: Positron annihilation spectroscopy is an important analytical method to detect vacancy-type defects and vacant spaces of materials. Energy-variable mono-energetic positron beams (slow positron beams) are essential to perform depth-dependent positron annihilation spectroscopy of surface layers such as ion-implanted layers or thin films formed on substrates. Intense positron sources are necessary to obtain slow positron beams for practical use. In general, positron sources based on pair creation can provide higher intensity than radioisotope-based positron sources. A positron source using pair-creation by gamma-rays from a nuclear reactor have been developed by using Kyoto University research Reactor (KUR) to obtain a slow positron beam for materials analysis. In the KUR slow positron beamline, the spot size at the sample chamber is more than 10 mm in diameter. To reduce spot sizes for smaller samples, a brightness enhancement system has been developed. Simultaneously, a lifetime measurement system based on a pulsing system using a radiofrequency-driven buncher was also developed for the KUR slow positron beamline [1]. In this report, the performance of the positron lifetime system was evaluated in comparison with the system at National Institute of Advanced Industrial Science and Technology (AIST).

EXPERIMENTS: Positron lifetime spectra of Kapton and H-implanted Si samples were measured at 6 keV by the KUR slow positron beam system. The same samples were measured at 6 keV by the AIST slow positron beam system. Among the samples, the results of the Kapton sample, as a reference material, were compared to understand the characteristics of the KUR system. The design of the pulsing system of the KUR system is based on that of the AIST system. The both systems use a combination of a transmission-type chopper and radiofrequency-driven buncher electrodes. Annihilation gamma-rays are detected by scintillation detectors using photomultipliers and BaF_2 crystals.

RESULTS: Figure 1 shows the lifetime spectra of the Kapton sheet measured at KUR and AIST systems. Solid lines show the original (as-measured) spectra. Dots show the spectra after back-ground subtraction. As described in the previous study [1], the KUR lifetime measurement system is influenced by background radiation, leading to the higher background signals even with the use of background discrimination circuits. A big satellite peak around 8 ns corresponds to the buncher signal and it was not sufficiently cut by the chopper electrode. Except for this chopper-origin peak, irregular background signals were treated as a part of the resolution function. In the case of the AIST spectra, the resolution function was calculated using a YSZ (yttoria stabilized zirconia) spectrum and then it was applied for the Kapton analysis. A broad satellite peak around 12 ns can be attributed to backscattered positrons. It is interesting to note that the different lifetime measurement systems have different background shapes like fingerprints. The spectrum analysis was performed assuming a single lifetime component. The lifetimes obtained for Fig.1(a) and 1(b) were 0.3815±0.0008 and 0.3805±0.0005 ns, respectively. These values are reasonably in agreement with previously reported Kapton lifetimes.

In summary, positron lifetime measurements were performed for several samples using the KUR and AIST slow positron systems. The levels and shapes of the background signals were different but both of Kapton lifetimes were reasonably in agreement with the previously reported values.

REFERENCES:

[1] M. Nakajima *et al.,* Rev. Sci. Instrum., **91** (2020) 125109.

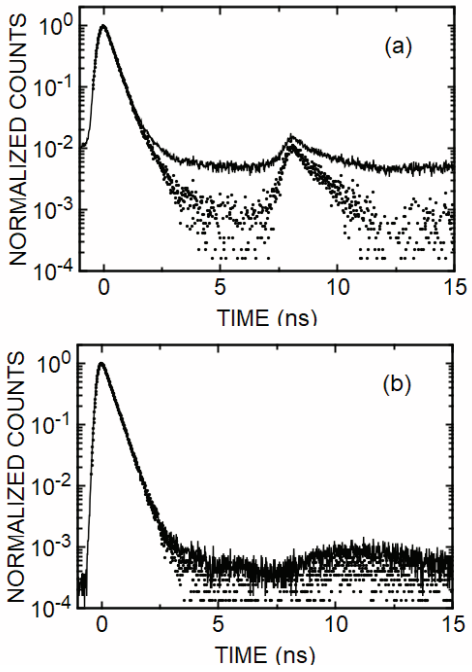

Fig. 1. Positron annihilation lifetime spectra of a Kapton sheet measured at (a) KUR and (b) AIST systems. Solid lines and dots show the original and background-subtracted spectra.

CO4-17 Complex Structure of Ions Coordinated with Hydrophilic Polymer 23. Iodine Doping with Organic Tissues.

A. Kawaguchi and, Y. Morimoto

IIRNS, Kyoto University (KURNS)

INTRODUCTION:

We have been investigating dynamical and interacted structures between iodine and polymers. Here, the term of "iodine" is not only simple iodine, I_2, but *polyiodide ions* (I_n^{m-}, *m, n*: integer, $n > 1$, "Poly-Iod(s)" mentioned below) as charged molecules, which suggest concealed potential and diverse availability for application with polymeric materials. [1,2]

"Poly-Iod"s are defined as charged molecules which are composed only by (more than one) iodine atoms as an unique element. They indicate spatial occupation, anisotropic molecular shapes, charge conjugation on molecule(s), chained structure between "Poly-Iod"s themselves through "halogen bonding (iodine bonding) ", variable distances between iodine atoms, etc; these singular behaviors are attributed to iodine as the characteristic element.

On the other hand, iodine atoms can often coordinate with other elements through lone pairs of electrons due to since its higher atomic number (Z=53). Additionally, even dipole or distributed positive charge (σ-hole) on "Poly-Iod" can be localized corresponding to their bonding with other atoms or ions. Or, though iodine is a member of halogen, mono-iodide ion, I^+, can behave as single cation with positive charge, while it does not belong to definition of "Poly-Iod". [3,4]

Such ambiguous and variable nature of "Poly-Iod" let be expected to introduce general affinity with variable polymeric structure in which dipole interaction potentially exist even whether the host polymer is hydrophilic or hydrophobic. If so, there can be expected novel functionality applied with interaction of "Poly-Iod"s with organic textures while they may not be paid attention as matrices for coordination nor be considered with hydrophilicity. [5]

EXPERIMENTS:

As host polymer originated organic texture, spallation of human throat (sputum) was sampled. As an aqueous solution of "Poly-Iod", I_2-KI(aq)/0.1N was prepared; 0.05M I_2 and 0.15M KI were solved in water. The samples were (1) casted and dried on a cover glass at first and immersed into following I_2-KI(aq)/0.1N, or (2) immersed into the solution at first and casted and dried on a cover glass (casting iodine-doped sputum on a glass substrate). After iodine doping, the samples were not rinsed with water. Mass deviation on each drying or doping process was not measured. While WAXD for the samples were observed through the cover glasses with penetrating MoKα radiation, spacing was not estimated.

RESULTS AND DISCUSSION:

While present results are not adequate for quantitative estimation, here may be hinted modification of organic tissues applied with "Poly-Iod(s)" solution.

The sampled sputum is decomposed collagen which is not polymeric material in macroscopic scale; it was solved and dispersed in water easily and was colorless.

Both process, iodine-doping after "drying and casting" and "drying and casting" after doping, indicated iodine adsorption explicitly in macroscopic observation; interacted coordination is actually realized between collagen as organic tissues and "Poly-Iod(s)". (Fig.1) [5]

On the other hand, microscopic behavior indicated in WAXD showed difference between the samples. Both samples showed arcs on diffraction; they suggested crystalline structure with host matrices (polymer or oligomer) since these diffraction (indicated with red arrows in Fig.1's) had sharp peak widths and anisotropic (?) orientation. Additionally, preceding iodine doping (Fig.1(b)) introduced other diffraction as oriented spots..

It is not clarified yet if these spots are attributed to coordinated structure between polymeric matrices and "Poly-Iod(s)" or to precipitation of low molecular substances independent of polymeric coordination. Nevertheless, arcs observed in diffraction are suggesting that iodine doping can introduce novel structure and application through interaction within organic tissues which have not been regarded as fields for functionality.

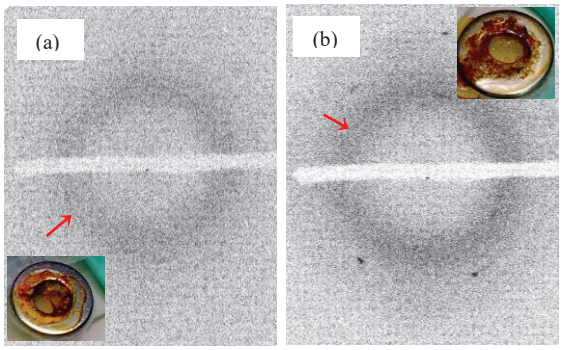

Fig.1: Adsorption as macroscopic observation and WAXD patterns indicating microscopic interaction of "Poly-Iod(s)" with collagen; (a) iodine doping after drying and (b) iodine doping before drying and casting.

REFERENCES:

[1] patent. JPN-5444559 (2014).
[2] "Projects for Practical Use from Innovation" sponsored by NEDO (2007-2009).
[3] T.J. Marks & D.W. Kalina, "Extended Linear Chain Compounds" vol.1 ch.6., ed. J.S. Miller (Plenum Press, 1982).
[4] T. Clark, *et.al.,* J Mol. Model, **13** (2007) 291-296.
[5] A. Kawaguchi, SPSJ Workshop, "58th KOHBUNSHI TO MIZU (Polymer and Water)" (on-line), (2020)1-2.

CO4-18 Chemical form of tritium released from neutron-irradiated FLiNaK mixed with Ti powder

K. Katayama, K. Kubo, T. Ichikawa, K. Masuta, M. Oya, T. Takeishi[1], K. Akashi[1], and Y. Iinuma[2]

Interdisciplinary Graduate School of Engineering Sciences, Kyushu University
[1]Faculty of Engineering, Kyushu University
[2]Institute for Integrated Radiation and Nuclear Science, Kyoto University

INTRODUCTION: As an advanced blanket concept of a DT fusion reactor, the self-cooling liquid blanket has been proposed. In this concept, primary cooling media plays two important roles of tritium transport and heat transport. Fluoride molten salts such as FLiNaBe and FLiBe are a promising liquid blanket material due to high stability at high temperatures, low reactivity with O_2 and H_2O, and low MHD pressure drop. Tritium is produced in the molten salts by the nuclear reaction between neutrons and Li. Since fluoride molten salts have a low solubility for hydrogen isotopes, the produced tritium tends to release from the molten salt. This property means that tritium can be easily recovered from the molten salt but also parts of tritium is lost to the outside of cooling tubes by the permeation on the way to the tritium recovery system. For suppressing tritium loss by increasing effective solubility for tritium, the addition of Ti powder was proposed [1]. However, few studies on molten salt materials containing Ti powder have been performed. In order to discuss the design of tritium recovery system, it is necessary to understand the fundamental behavior of tritium in the molten salt mixed with Ti powder. Since FLiNaBe and FLiBe contain highly toxic beryllium and is not easy to handle safety, FLiNaK is usually used as a simulated fluid. In this study, the solid state sample of FLiNaK mixed with Ti powder was irradiated by neutrons at Kyoto University Research Reactor, and the chemical form of tritium released from the free surface of the molten salt by heating was observed in Kyushu University.

EXPERIMENTS: In the powders of LiF, NaF and KF were mixed in a Ni crucible under Ar atmosphere. The Ni crucible was put in the stainless-steel heating pot and repeatedly heated to 600 ℃ with Ar purging to remove impurity water vapor. The heating was repeated to homogenize the FLiNaK and the plateau region of temperature change was confirmed at 454 ℃ which is melting point of FLiNaK. A part of FLiNaK was sampled for the measurement of water vapor by heating in Ar gas flow.

Ti powder was added to the part of FLiNaK with 2.5 wt% and it was heated with Ar purging. The prepared sample of FLiNaK was packed into quartz tubes in vacuum and it was installed into a polyethylene capsule. The thermal neutrons irradiation was performed by at pneumatic tube 2 (Pn-2) with the fluence of at Pneumatic Tube 2 (Pn-2) of the 1.7×10^{15} cm^{-2}.

The release behavior of water vapor from non-irradiated FLiNaK without Ti was investigated by heating at 600 ℃ in Ar gas flow with 400 cc/min. The concentration of water vapor in the outlet gas was monitored with a hygrometer (MAH-50, SIMAZU Co.). The FLiNaK granules were put in a Mo crucible and it was installed in a quartz reaction tube.

Tritium release experiment was carried out for neutron irradiated FLiNaK. The irradiated sample was put in a Mo crucible and it was installed in the quartz reaction tube. In order to melt the sample sufficiently, heating temperature was set to be to 600 ℃ or 700 ℃ with Ar purge. The chemical form of tritium released from the sample was expected to be TF, T_2 and T_2O, and these were separately quantified. Details of the quantification method were described in Ref.2.

RESULTS: The release behavior of water vapor from the FLiNaK is shown in Fig.1. Two release peaks were observed in the water vapor release curve. It is considered that the first peak is caused by the desorption of water vapor adsorbed on the surface of FLiNaK granules and the second peak is caused by the desorption contained in the bulk of FLiNaK. From the amount of released water, the concentration of water in FLiNaK including surface adsorbed water was estimated to be 1.44 wt %.

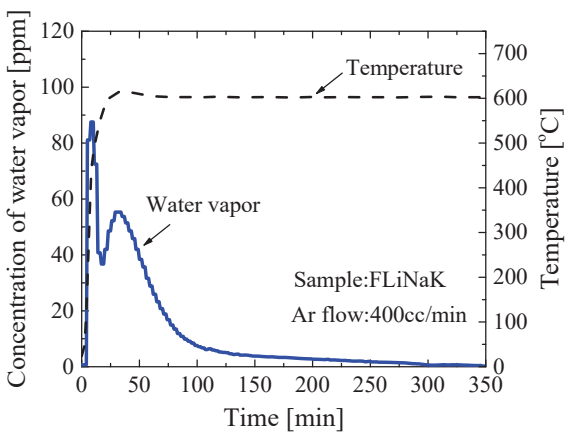

Fig.1. Water vapor release from non-irradiated FLiNaK without Ti.

It was found that about 70 % of tritium was released as T_2 and about 25 % of tritium was released as T_2O, and about 5 % of tritium was released as TF. It can be said that since the FLiNaK sample used in this experiment contained a relatively high concentration of water of 1.44 wt%, about 25 % of tritium was released as T_2O. In the Ar gas purge during FLiNaK preparation process, if the water vapor concentration in the outlet gas is measured and sufficient water vapor desorption is performed, the release ratio of T_2O is expected to be reduced.

REFERENCES:

[1] A. Sagara *et al.,* Fusion Eng. Des., **89** (2014) 2114.
[2] K. Kubo *et al.,* Fusion Eng. Des., **171** (2021) 112558.

CO4-19 Study on ^{99m}Tc separation/concentration technology from ^{99}Mo by (n, γ) method

Y. Fujita, X. Hu[1], T. Takeuchi, R. Takeda, Y. Fujihara[2], H. Yoshinaga[2], J. Hori[2], T. Suzuki[1], H. Suematsu[1] and H. Ide

Department of JMTR, Japan Atomic Energy Agency
[1]Graduate School of Engineering, Nagaoka University of Technology
[2]Institute for Integrated Radiation and Nuclear Science, Kyoto University

INTRODUCTION: Study on the production of molybdenum-99 (^{99}Mo) by the (n, γ) method has been carried for the domestic production of technetium-99m (^{99m}Tc) without using uranium. Technology to concentrate ^{99m}Tc, a daughter nuclide of ^{99}Mo, is required because the specific activity of ^{99}Mo produced by this method is low. We focused on a technique to extract ^{99m}Tc by solvent extraction using methyl ethyl ketone (MEK) and to concentrate it by alumina columns [1]. Since it has been reported that reduced ^{99m}Tc is not extracted into MEK [2], it is necessary to investigate the effect of ^{99m}Tc reduction on ^{99m}Tc yield. In this work, we attempted to reduce ^{99m}Tc by bubbling hydrogen into sodium molybdate solution (Mo solution) and investigated the effect on the yield. In addition, Raman spectroscopy of the collected ^{99m}Tc solution was performed as basic data for identifying the chemical form of ^{99m}Tc.

EXPERIMENTS: MoO_3 pellet pieces (1.5 g) were irradiated in Pn-2 at 5 MW for 20 min and dissolved in 6M-NaOHaq. This solution was mixed with non-irradiated Mo solution. The ^{99m}Tc extraction process was carried out for 3 days and the Mo solution was used repeatedly.
First, on days 1 and 3 only, the Mo solution was hydrogen bubbled for an hour using hydrogen generation by dissolving aluminum pieces in 6M-NaOHaq. Fifteen mL of MEK and the Mo solution were added to a separatory funnel and shaken for 3 min to extract ^{99m}Tc into MEK. Both solutions were stood for 3 min and separated. The separated MEK was passed through a basic column (basic alumina: 1 g) to remove the small amount of Mo solution. Second, 10 mL of fresh MEK was flowed through the basic column to remove ^{99m}Tc remaining in the column. The two MEKs were mixed and poured into an acidic column (acidic alumina: 1 g) to adsorb ^{99m}Tc onto the column. The acidic column was washed with 30 mL of deionized water to remove MEK. Finally, 10 mL of saline was flowed through the acidic column to elute ^{99m}Tc. The activity of the solutions obtained in each process was measured by γ-ray spectrometer.
Raman spectroscopy analyzed a decayed ^{99m}Tc solution (about 445 pg-Tc/mg) using a laser with an excitation wavelength of 785 nm.

RESULTS: The ^{99m}Tc content in the substance for each process was shown Fig. 1. The ^{99m}Tc content is the ratio of the ^{99m}Tc amount in each substance to the one in the Mo solution just after extraction. The activity of ^{99m}Tc in the Mo solution was calculated from the one of ^{99}Mo. The activity of ^{99m}Tc was decay corrected based on the start of extraction. The results showed a clear decrease in ^{99m}Tc adsorption rate on an acidic column only on the days 1 and 3, in which the Mo solution was hydrogen bubbled. In contrast, the effect on ^{99m}Tc extraction to MEK reported in the paper was not confirmed. Therefore, it was shown that hydrogen bubbling into Mo solution didn't affect ^{99m}Tc extraction to MEK but may interfere with ^{99m}Tc adsorption to an acidic column. However, since the chemical form of ^{99m}Tc has not been determined, further experiments are needed to determine if ^{99m}Tc reduction is the cause.

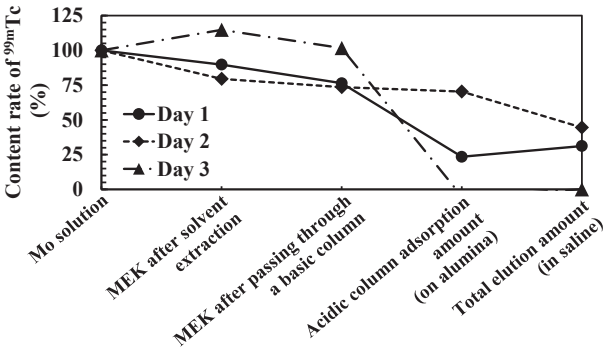

Fig. 1. ^{99m}Tc content in each process.

The Raman spectrum of ^{99m}Tc solution is shown in Fig. 2. The upper figure shows the superimposed spectra of the ^{99m}Tc solution and the saline, and the lower one is the spectrum created by subtracting the saline one from the ^{99m}Tc solution one. A sharp and weak peak at around 1050 cm^{-1} was observed. This peak is assumed to be the Raman peak of TcO_4^-. In the future, we will investigate the difference of the Raman peak due to the chemical form of Tc and so on.

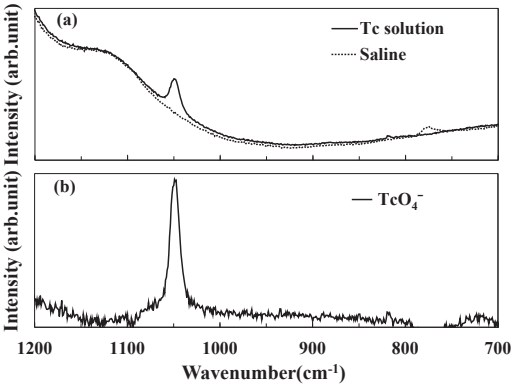

Fig. 2. Raman spectra; (a) Tc solution and saline (b) TcO_4^-

REFERENCES:

[1] S. Chattopadhyay *et al.*, Appl. Radiat. Isot., **68** (2010) 1-4.
[2] R. E. Boyd *et al.*, Radiochim. Acta, **30** (1982) 123-145.

CO4-20 Observation of Low Fluence Irradiated Accident Tolerant Control Rod Material

H. Ohta[1], K. Nakamura[1], Y. Takahashi[2], H. Unesaki[2]

[1]*Energy Transformation Research Laboratory, Central Research Institute of Electric Power Industry*
[2]*Institute for Integrated Radiation and Nuclear Science, Kyoto University*

INTRODUCTION: Various concepts of enhanced-accident tolerant fuels and core components have been developed to improve core safety under any operation conditions including severe accidents (SAs), while maintaining or improving the economic efficiency of light water reactors (LWRs). Central Research Institute of Electric Power Industry has been developing the accident tolerant control rods (ATCRs) where the novel neutron absorbing materials including rare-earth oxides (RE_2O_3) are applied[1] to prevent control rods (CRs) from damaging prior to fuel rods in the early stages of SAs. Preliminary analyses [1] revealed the ATCRs can improve the reactor shutdown margin and neutronic lifetime. RE_2O_3 (RE=Sm or Eu) has excellent high temperature compatibility with the stainless steel of CR cladding, and is not damaged less than 1200 °C [2, 3]. On the other hand, RE_2O_3 is known to be highly hygroscopic and chemically unstable, but it was experimentally confirmed that physicochemical stability is improved even under high temperature steam atmosphere by mixing and sintering with MO_2 (M=Zr or Hf) [3]. In addition, it is necessary to confirm the neutron irradiation stability of RE_2O_3-MO_2 to evaluate its applicability as an ATCR material. For that purpose, irradiation experiments of Sm_2O_3-ZrO_2 with neutron fluences of 2.39×10^{19} n/cm^2 and additional 2.13×10^{19} n/cm^2 have been completed by 2020. Then, postirradiation observations of the Sm_2O_3-ZrO_2 samples irradiated up to a total fluence of 4.51×10^{19} n/cm^2 will be performed in this study.

EXPERIMENTS and RESULTS

Sample Preparation: The powders of Sm_2O_3 and ZrO_2 were mechanically mixed at a molar ratio of 1 : 1 and sintered to form a pellet with a density of 6.55 g/cm^3 corresponding to 93.7 %TD. Since any sintered mixture of RE_2O_3 and MO_2 (RE = Sm or Eu, M = Zr or Hf) with a molar ratio of 1 : 1 forms a fluorite-type crystal structure, the results of irradiation experiments with Sm_2O_3-ZrO_2 samples are considered to be applicable to the other combination materials. To reduce the radioactivation induced by the neutron irradiation as low as possible, the sintered pellet was cut into small pieces. The appearance and surface microstructure of the cut sample pieces before irradiation was observed with an optical microscope and scanning electron microscope (SEM), and their weights were measured.

Irradiation Conditions: Two campaigns of irradiation experiment were carried out using long-term irradiation plug in Kyoto University Research Reactor (KUR). Three Sm_2O_3-ZrO_2 sample pieces were enclosed in an Al capsule dedicated for long-term irradiation experiment. The irradiation periods were 530.7 hours in the 1st campaign and 475.2 hours in the 2nd campaign at an equivalent reactor power of 1 MW. The irradiation temperature in the long-term irradiation plug is pre-evaluated as 85-90 °C. The neutron fluences at the end of 1st and 2nd irradiation experiments are evaluated to be 2.38×10^{19} n/cm^2 and 4.51×10^{19} n/cm^2, respectively, which is almost equivalent to irradiation fluence for 1-1.5 days in typical PWRs.

Postirradiation observations: After cooling for each irradiation campaign, the appearances of the irradiated samples were observed, and their weights were also measured. The results of weight measurement before and after irradiations were shown in Table I. No systematic weight change was observed between the 1st and 2nd irradiations in these samples. Although the smallest sample (1) showed a maximum weight change of about 3% (0.06 mg) during 2nd irradiation, it was confirmed that there was no significant weight change considering the measurement accuracy of ± 0.05 mg. Figure 1 shows the appearance of each sample before irradiation and after 2nd irradiation. No changes in the appearance and the dimensions due to neutron irradiation were confirmed.

Table I. Weight changes of Sm_2O_3-ZrO_2 samples before and after irradiation [4].

Sample No.	(1)	(2)	(3)
Before irradiation	1.95 mg	6.21 mg	5.15 mg
After 1st irradiation	1.97 mg	6.15 mg	5.11 mg
After 2nd irradiation	1.91 mg	6.24 mg	5.16 mg

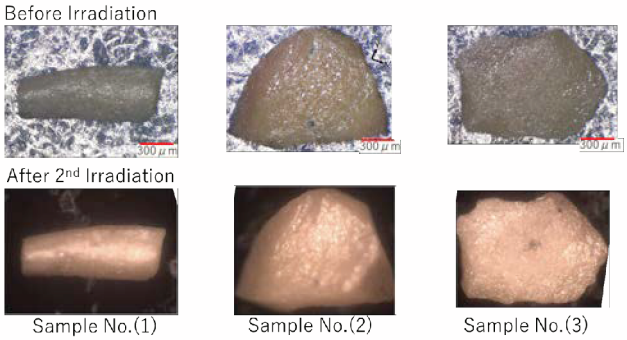

Fig. 1. Optical micrographs of Sm_2O_3-ZrO_2 samples before irradiation and after 2nd irradiation.

CONCLUSION: Postirradiation observations of sintered Sm_2O_3-ZrO_2 samples irradiated in KUR showed that the no significant changes occurred in the weight and dimensions of the ATCR neutron absorbing materials under a neutron fluence of 4.51×10^{19} n/cm^2.

REFERENCES:

[1] H. Ohta *et al.,* TopFuel 2016, (2016).17556.
[2] K. Nakamura *et al.,* AESJ 2017 spring meeting, 1I06.
[3] K. Nakamura *et al.,* 27th Int. QUENCH Workshop, (2022).
[4] H. Ohta *et al.,* NuMat 2022, O1.5 (2022).

CO4-21 Evaluation of Irradiation Damage on Semiconductor Surfaces during Plasma Etching using the Positron Annihilation Method

J. Yanagisawa, R. Shigesada, Q. Xu[1], A. Yabuuchi[1], K. Takamiya[1], and A. Kinomura[1]

School of Engineering, The University of Shiga Prefecture
[1]*Institute for Integrated Radiation and Nuclear Science, Kyoto University*

INTRODUCTION: We have been studying the ion irradiation-induced damage on semiconductor surfaces using the positron annihilation method. In our previous report [1], to study the effect of the ion-irradiation induced damage at lower ion energy and lower ion fluence, SF_6 plasma-exposed Si wafer chips were investigated. It is found that damages, such as vacancies and voids, were induced inside Si surfaces after the etching by the SF_6 plasma treatment. In the present study, another gas species, such as CHF_3 and Ar, were used to form the plasma, and damages inside Si surfaces induced by such plasma treatment were investigated using the positron annihilation method.

EXPERIMENTS: Chips cleaved from Si (100) wafer with the size of 18 mm x 18 mm were used in the present study. After wet cleaning using acetone and 2-propanol, the samples were exposed to RF plasma at a power of 5 W with a gas pressure of 30 Pa using SF_6 (sample number: #6), CHF_3 (#8), or Ar (#10) gas. No plasma exposed sample (#1) was also used as a reference of bulk Si. S parameters and life time spectra of the positrons for the Si samples were measured using slow positron beam system (B-1) in KUR at beam energies of 0 – 30 keV.

RESULTS AND DISCUSSION: Fig. 1 shows the S parameters for the samples as a function of the incident positron energy. Fig. 2 shows the spectra of the life time of positrons in the Si samples. In Fig. 1, S parameters near the surface region (positron energy: 0 – 15 keV) of the samples #6 and #10 were larger than that of un-treated Si (#1), indicating that the damages were induced by SF_6 and Ar plasma. However, that of the sample #8 was smaller than that of Si (#1). Although resemble behavior was observed for BF_2^+ ion implanted Si [2], the reason for the reduction of the S parameter from the bulk Si is not known at present. However, the life time of the positrons of 401.7 ns (#6), 466.8 ns (#8) and 444.4 ns (#10), which were calculated using Fig. 2, were larger than that of the bulk Si (218.1 ns (#1)), indicating the formation of damages by the plasma treatment.

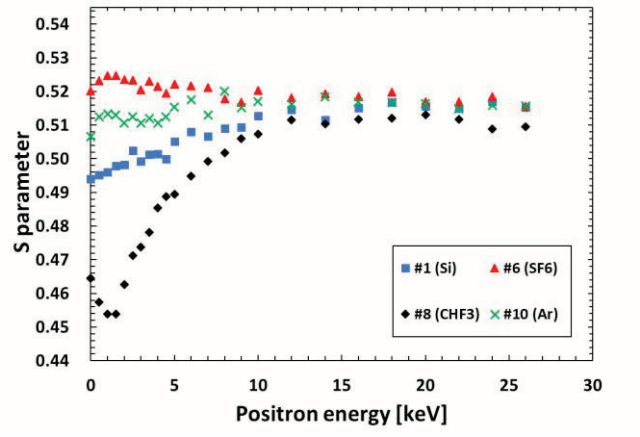

Fig. 1. S parameters for plasma treated (#6(SF_6), #8(CHF_3), #10(Ar)) and untreated (#1) Si wafer samples as a function of positron energy. The introduced gas pressure of 30 Pa and the RF power of 5 W were used to form each plasma.

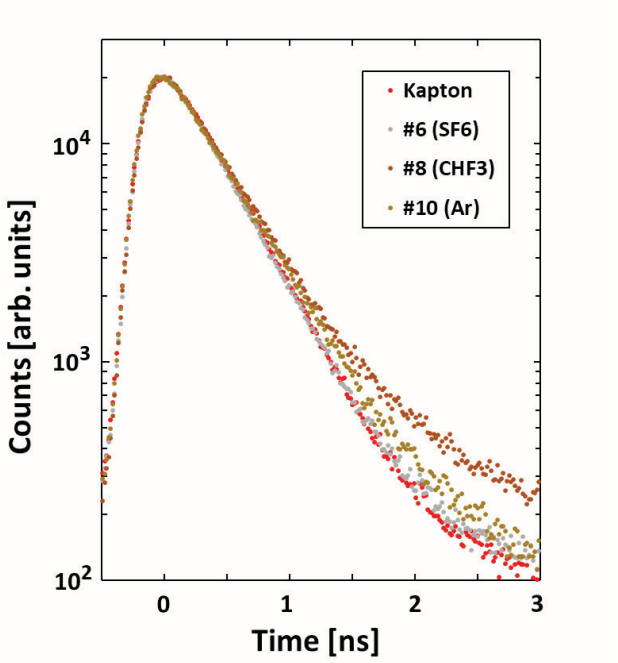

Fig. 2. Life time spectra of positrons in plasma treated (#6, #8, and #10) Si wafer samples measured at 1 keV. The result for a Kapton film is also shown as a reference.

CONCLUSION: Although the effects of the plasma on Si using SF_6, CHF_3 or Ar gas might be different from each other, it is found that damages were induced by the plasma treatment. The difference of the effects using different gases for the plasma formation should be clarified.

REFERENCES:

[1] J. Yanagisawa *et al.*, KURNS Progress Report 2021 (Kyoto University), CO4-11 (R3078).
[2] A. Uedono *et al.*, Jpn. J. Appl. Phys. **36** (1997) 969.

CO4-22 Correlation between irradiation defect density and hydrogen isotope retention in tungsten

M.I. Kobayashi[1,2], N. Abe[3] and T. Takahashi[3]

[1]*National Institute for Fusion Science, National Institutes of Natural Sciences*
[2]*The Graduate University for Advanced Studies, SOKENDAI*
[3]*Institute for Integrated Radiation and Nuclear Science, Kyoto University*

INTRODUCTION: In a deuterium-tritium (D-T) fusion reactor, tungsten (W) will be exposed to energetic particles such as fast neutrons. By the collision of these energetic particles, W atoms in the lattice points are displaced to form irradiation defects. Hydrogen isotopes are trapped in the irradiation defects, leading to a loss of fuel in the reactor. A previous study showed about two orders of magnitude larger deuterium retention in neutron irradiated W compared to non-irradiated W [1]. In addition, the deuterium desorption temperature shifted higher in neutron-damaged W. These results suggest that irradiation defects trapped hydrogen isotopes, and consequently, the retention and the desorption behaviors of hydrogen isotopes in W drastically changed. Therefore, this study aims to evaluate the quantitative correlation between irradiation defect density and hydrogen isotope retention in W irradiated with electron beam which can introduce only point defects.

EXPERIMENTS: The W sample was purchased from Nilaco co. The thickness of the sample was 25 μm. A sample was annealed at 1173 K for 6 hours under the pressure below 10^{-5} Pa (The annealed W) at National Institute for Fusion Science (NIFS). Then, samples were shipped to KURNS-LINAC for electron irradiation. The electron acceleration voltage was 8 MV. The dose was evaluated as 4.3×10^{-3} dpa according to an atomic displacement cross-section of 70.4 barns and a displacement threshold energy of 84 eV [2]. The irradiation temperature was less than 353 K due to the water coolant.

For the evaluation of the interaction between hydrogen isotopes and irradiation defects in W, the deuterium gas permeation system was prepared in NIFS. A disc shaped thin metal samples can be mounted to separate the vacuum system in this device. A side of the vacuum system can be filled with deuterium gas with desired pressure and temperature (upstream side). Another side of the system is evacuated by a turbo molecular pump (downstream side), and the desorption of permeated deuterium was monitored by a quadrupole mass spectrometer.
As the benchmark experiment, we used a nickel (Ni) foil with the thickness of 50 μm. Then, the W samples were examined. We report here the results on the annealed W and the as-received W (un-annealed W).

RESULTS: Figure 1 shows the summary of deuterium permeability in Ni as a function of the reciprocal temperature. The deuterium permeability increased exponentially with the elevated temperature. The permeation processes of hydrogen isotopes consist of diffusion and solution processes. The rates of these processes vary with the temperature according to the Arrhenius's law. Therefore, the deuterium permeability has the exponential temperature dependency.

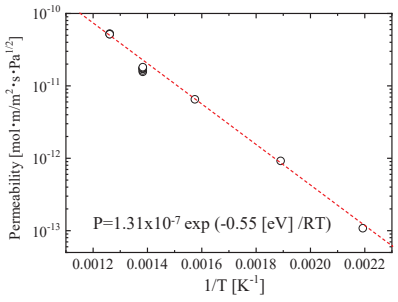

Fig.1. Deuterium permeability in Ni.

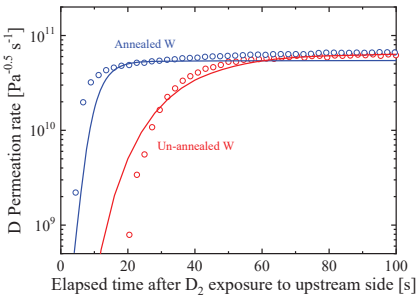

Fig.2. Time evolution of deuterium permeation flux in annealed W and un-annealed W.

Figure 2 shows the transient curves of deuterium permeation flux in W samples after the beginning of deuterium gas exposure to the upstream side. A gradual increase of deuterium permeation flux and a subsequent steady-state permeation flux comes from the evolution of deuterium distribution in W samples. It can be seen that the annealed W achieved a steady-state deuterium permeation quickly compared to the unannealed W. This indicates the trapping effects of diffusing deuterium by defects in W which apparently decrease the deuterium diffusion rate in W. Using a simulation code in which the diffusion behavior of hydrogen isotopes with competitive trapping/detrapping processes in W can be solved [3], the deuterium permeation fluxes for these samples were analyzed, and the deuterium permeation curves were roughly reproduced as found in Fig. 2. From this analysis, the trapping site density for annealed W was evaluated to be 1.5×10^{-3} at.%, besides, that in un-annealed W was 3.5×10^{-3} at.%. We will perform the similar series of experiments for electron irradiated W, and the increase of the trapping site density will be estimated.

REFERENCES:

[1] Y. Hatano *et al.*, Nucl. Fusion, **53** (2013) 073006.
[2] K. Sato *et al.,* Nucl. Mater. Ene., **9** (2016) 554.
[3] M.I. Kobayashi *et al.*, Fusion Eng. Des., **168** (2021) 112635.

CO4-23 Characteristics of Improved Tetrode Configuration for Radiation Tolerant Image Sensor

Y. Gotoh, Y. Neo[1], M. Nagao[2], and N. Sato[3]

Graduate School of Engineering, Kyoto University
[1]Research Institute of Electronics, Shizuoka University
[2]National Institute of Advanced Industrial Science and Technology, AIST
[3]Institute for Integrated Radiation and Nuclear Science, Kyoto University

INTRODUCTION: In decommissioning of Fukushima Daiichi Nuclear Power Plant, observation of inside of the reactor pressure vessel is one of the most important issues. We have been developing an image sensor based on field emitter array (FEA), which is a two-dimensional miniaturized electron source. Radiation tolerance of the components of this image sensor has already been demonstrated [1]. Last year, light-detection test under γ-ray irradiation was attempted with a proto-type image sensor, and it was found that the device yielded a small signal of light even under γ-ray irradiation [2]. The signal was very weak, and one of the reasons would be the electrode configuration of the image sensor; the distance between the FEA and the anode which accumulates photo-signal was too large. In this study, some of the metal and insulator plates which supported the mesh electrode and photoconductor were eliminated in order to locate the anode much closer to the FEA. With the improved configuration, the characteristics of the device was investigated with and without γ-ray irradiation.

EXPERIMENTS: The image sensor consisted of an FEA, mesh, and anode. The FEA used in this study was the identical one to the previous experiment [3]. In the previous experiment, the mesh was fixed with two 1 mm-thick metal plates, and the photo-conductor was also fixed in a similar way to the mesh. Between the mesh and the photoconductor, a 1 mm-thick insulting plate was inserted to maintain the gap of the electrodes. In the present device, the mesh was spot-welded to a 1-mm thick metal plate, and the anode was set close to the mesh without using an insulating layer. The distance between the mesh and the photoconductor in the previous study, and that between the mesh and a metal anode was reduced more than 2 mm. The device was installed in the identical vacuum vessel used in the previous study. A non-evaporative getter pump was activated to evacuate the vessel. The pressure before the experiment was less than 1 x 10^{-6} Pa. The FEA used in the present study was the same one as used in the present study [3]. The emitter was grounded, and the gate was positively biased between 46 and 50 V. The mesh electrode was biased to 200 V. The mesh current ranged from 2.5 μA to 7 μA. The emitter current could not be measured due to circuitry problem. The anode characteristics were acquired varying the anode voltage 0 to 60 V with and without γ-ray irradiation. The dose of irradiation was estimated to be 410 Gy h^{-1} at the anode plate.

RESULTS: Figure 1 shows anode characteristics with and without γ-ray irradiation. The gate potential was 50 V. The abscissa is the anode voltage and the ordinate is the anode current. The solid and open circle indicate the characteristics with and without γ-ray irradiation, respectively. The anode current began to increase at 10 V. The anode current showed a maximum at 20 V, and then turned to decrease. The maximum anode current without γ-ray irradiation was 1.2 μA, which is sufficient to act as an image sensor. At the gate voltage of 46 V, the maximum anode current was 600 nA. The increase of the anode current would be attributed to the reduction of the decelerating electric field between the mesh and the anode. The decrease of the anode current higher than 20 V would be attributed to the increase of the secondary electron emission coefficient due to higher incident energy of electrons. The anode characteristics showed little difference with γ-ray irradiation. Slight difference is due to the difference of the beam current, which was proven from the anode current normalized by the mesh current showed a good agreement. It was already shown that γ-ray irradiation with the dose rate of irradiation of higher than 1 kGy h^{-1} did not affect the characteristics of the triode [4]. The present result indicated that the newly constructed device configuration realized sufficient anode current, and the performance was not affected by the γ-ray irradiation. The effect of γ-ray irradiation to the photo-detection performance will be tested in the following experiments.

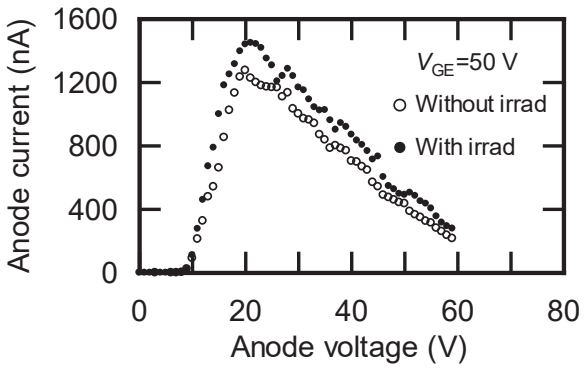

Fig. 1. Anode characteristics with and without γ-ray irradiation.

REFERENCES:

[1] Y. Gotoh *et al.*, IEEE Trans. ED, **67** (2020) 1060-1065.
[2] Y. Gotoh *et al.*, KURRI Progress Report 2021, (2022) CO4-8.
[3] T. Sato *et al.*, J. Vac. Sci. Technol. B, **21** (2003) 1589-1593.
[4] T. Morito *et al.*, IEEE 31st International Vacuum Nanoelectronics Conference, Kyoto, July 9-13, 2018 (2018) 96-97.

CO4-24 Characterization of $YBa_2Cu_3O_y$ and $FeSe_{0.5}Te_{0.5}$ superconducting films using a slow positron beam

T. Ozaki, H. Sakane[1] and A. Yabuuchi[2]

School of Engineering, Kwansei Gakuin University
[1]SHI-ATEX Co., Ltd.
[2]Institute for Integrated Radiation and Nuclear Science, Kyoto University

INTRODUCTION: Cuprate and iron-based superconducting films are expected for magnet applications in areas of basic science, medicine and levitation. For these applications, raising critical current, which is a maximum value of zero-resistivity current, property in magnetic fields is very important. The critical current in applied magnetic fields could be improved by introducing structural defects with nano-meter size using ion-irradiation techniques. Positrons are sensitive to vacancy-type defects, and they are useful for characterizing irradiation-induced defects. In this study, we probed two kinds of pristine superconducting films, cuprate superconductor $YBa_2Cu_3O_y$ (YBCO) and iron-based superconductor $FeSe_{0.5}Te_{0.5}$ (FST), using a slow positron beam, so that we will evaluate the irradiation defect in these films using the positron annihilation measurement.

EXPERIMENTS: The YBCO and FST thin films were deposited on $SrTiO_3$ (STO) single crystal substrates by pulsed laser deposition (PLD) method using a Nd:YAG laser (λ = 266 nm). These films were probed by the KUR slow positron beam and the Doppler broadening of annihilation radiation (DBAR) spectra were acquired with incident positron energies E_+ = 9 keV. The sharpness of the DBAR spectra is evaluated by a value called the *S*-parameter, which becomes generally lower when positrons annihilate in a perfect lattice, and higher when positrons are trapped into vacancies [1].

RESULTS: Fig. 1 shows the *S*-parameters of the YBCO thin film as functions of the incident positron energy. For higher implantation energies $E_+ > 7$ keV, a fraction of positrons annihilates in the STO substrate whereas for $E_+ < 4$ keV positrons also annihilate at the film surface. The *S*-parameters in the energy region of 4−7 keV correspond to positron annihilation in the YBCO layer. The low *S*-parameters at 4−7 keV could indicate that the YBCO layer contains a low concentration of vacancy-type defects. Fig. 2 shows the *S*-parameters of the FST thin film as functions of the incident positron energy. The *S*-parameters at 1−4 keV would be indicative of the positron annihilation in the FST layer. The *S*-parameter values in the FST layer is clearly higher than those in the STO substrate. This could be attributed to: (i) *S*-parameter values in the FST layer would be essentially higher than those in the STO substrate, or (ii) the vacancy-type defects would be formed in the FST layer during the film growth process. In order to determine whether which one is highly likely, we need to carry out first principle calculation on the *S*-parameters of each materials.

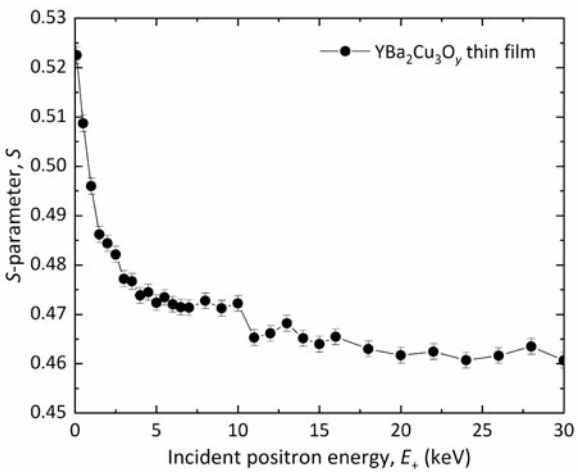

Fig. 1. *S*-parameters as functions of the incident positron energy for the $YBa_2Cu_3O_y$ thin film.

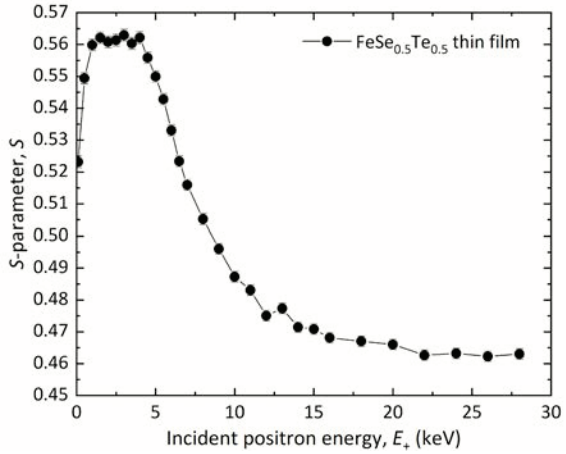

Fig. 2. *S*-parameters as functions of the incident positron energy for the $FeSe_{0.5}Te_{0.5}$ thin film.

REFERENCES:

[1] R. W. Siegel, Ann. Rev. Mater. Sci., **10** (1980) 393-425.

CO4-25 Neutron irradiation tests for components of ITER plasma diagnostics

M. Ishikawa, T. Ushiki, E. Yatsuka, K. Torimoto, M. Inamine, H. Murakami, K. Shimizu, T. Sugie, S. Kono and Y. Nunoya

National Institutes for Quantum Science and Technology

INTRODUCTION: ITER [1] is being built in France by international cooperation. Components of diagnostic systems installed in the ITER tokamak are exposed to high radiation. Therefore, it is important to investigate the radiation resistance of those components. In this study, neutron irradiation effects on optical elements such as lens and glasses used for Infrared Thermography system (IRTh) and Edge Thomson Scattering system (ETS) were investigated, respectively. The effects of neutron irradiation on an electronic device, the preamplifier of the Microfission chamber system (MFC), were also evaluated. Considering the neutron conditions at the installation location of the electronic device, the irradiation test was conducted at CN-3. Details are given below.

(1) Irradiation Tests of Si for Optical Lens of IRTh

IRTh is planning to use Si lenses in the ITER. The authors recently conducted separate gamma-ray and neutron irradiation tests. The gamma-ray irradiation test showed that the transmittance of Si is not significantly degraded in the wavelength range used by IRTh (1.5 μm - 4.5 μm). The neutron irradiation test showed that the transmittance of Si is not significantly degraded up to about 2.5 x 10^{15} (n/cm^2). However, no investigation has been conducted so far on the changes in refractive index due to irradiation. Change in refractive index could affect the chromatic aberration, focus position and optical performance of IRTh optics. Therefore, in this study, the authors investigated the changes in refractive index of Si before and after neutron irradiation tests.

EXPERIMENTS: For the irradiation test of Si samples, the slant exposure tube was used. Several Si samples were irradiated at multiple neutron fluences up to 1.0 x 10^{16} (n/cm^2). Refractive index measurement was taken at three wavelengths (3.35 μm, 4.19 μm and 4.45 μm) before and after neutron irradiation.

RESULTS: Fig. 1. shows the example of irradiation test result of Si samples. As shown in Figure 1, refractive index of Si decreased slightly due to neutron irradiation up to 1.0 x 10^{16} (n/cm^2). The impact on of the refractive index change on chromatic aberration, focus position, and opti-cal performance of IRTh will be quantitatively investigated in the future.

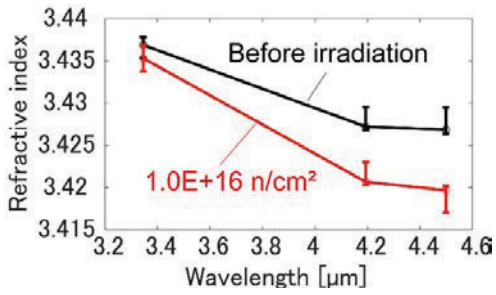

Fig. 1. Refractive index of Si before and after irradiation

(2) Irradiation Tests of Glass for compensating chromatic aberration of ETS

ETS will measure the spectrum at wavelengths of approximately 600-1060 nm to determine the electron temperature and density in the ITER fusion plasma. If the collection optics were constructed using only fused silica, the focal position would change for each wavelength due to the wavelength dependence of the refractive index (dispersion). Therefore, a glass material with a different refractive index and dispersion from fused silica is required. Cerium-doped glass, which is said to be durable against irradiation of cosmic rays including gamma rays, is considered promising. Estimated neutron fluence at the position where the glass is placed is of the order of 10^{16} (n/cm^2).

EXPERIMENTS: Cerium-doped glass called SF6G05 manufactured by Schott was irradiated up to 4x10^{15} (n/cm^2) for fast neutron and 2x10^{16} (n/cm^2) for thermal neutron, which is several times higher the 20-year cumulative fluence at the location of lens optics for ETS in ITER. The performance deterioration due to neutron irradiation was investigated by comparing the wavelength dependence of transmitted signal before and after irradiation.

RESULTS: Fig. 2. shows the spectral transmission of cerium-doped glass SF6G05 having the thickness of 10 mm before and after irradiation. In the end of 2021, deterioration in transmittance was observed in some samples, so a reproducibility test was performed. In February 2023, all the samples show the same tendency, and the decrease in transmittance is not remarkable at wavelengths above 600 nm, which is important for ETS. It is not clear why the results differed from those before. Perhaps the details of the manufacturing method, such as the heat history during glass molding and anti-reflection coating, are different.

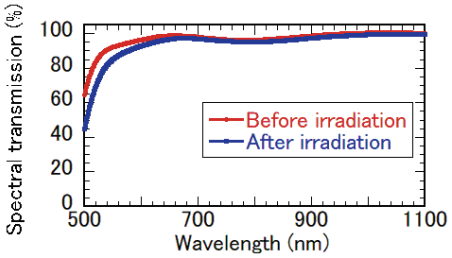

Fig. 2. Spectral transmission of cerium-doped glass (SF6G05) before and after irradiation

(3) Irradiation Tests of the preamplifier of MFC

The preamplifier of the MFC amplifies and converts a weak signal from the MFC detector into a nose tolerant strong output. The preamplifier will be installed in the port cell area and maximum neutron flux at the installation position of the preamplifier with neutron shielding could become about 2.4 x 10^3 n/cm^{2}s. However, the effects on neutrons have not been evaluated yet. Therefore, in order to investigate whether a preamplifier can be applied under the current shielding design. The neutron irradiation test on the preamplifiers was conducted at CN-3.

EXPERIMENTS: The preamplifier was installed near the conduit exit of CN-3 so that the semiconductor elements of the Preamplifier would be most exposed and neutrons were irradiated up to 1.0 x 10^{11} (n/cm^2), corresponding to neutron fluence for 20 years under the current shielding design. To properly investigate the effects of neutron irradiation, output power from the preamplifier, power consumption and temperature of the preamplifier were constantly monitored in situ during irradiation.

RESULTS: No change in output signal was observed, including no change in amplitude and no noise generation. On the other hand, a change in the current consumption of the preamplifier was observed, but this was consistent with the temperature, confirming that it was not due to neutron irradiation. This result suggests that the preamplifier can be used without replacement under its current design.

REFERENCES:

[1] B. Bigot, Fusion Eng. Des., **146** (2019) 124.

CO4-26 Study of resonant frequency change with irradiation dose of piezoelectric PZT element

M. Kobayashi, T. Miyachi, S. Takechi[1], Masaya Danjohbara[1] and Haruki Oh'ishi[1], Shoki Maeda[1], Shuhei Tominaga[1]

Planetary Exploration Research Center, Chiba Institute of Technology
[1]Graduate School of Engineering, Osaka Metropolitan University

INTRODUCTION: This study aims to establish an inexpensive method for dosimetry in high-dose environments. We consider changes in piezoelectric properties of piezoelectric elements due to irradiation for dosimetry in high-dose environments. For this purpose, the mechanism of radiation-induced change of piezoelectric properties has been investigated.

In a previous experiment conducted at NIRS/HIMAC, piezoelectric PZT elements were irradiated with 400 MeV/n Xe particles, and the decrease in the electromechanical coupling coefficient k was investigated [1][2]. As a result, it was found that k_r of the irradiated PZT element was -0.35%/kJ, which is a phenomenon concerning the irradiation dose [3]. In order to investigate what happens to piezoelectric elements due to irradiation, electron beam irradiation experiments have been conducted at KURNS-LINAC. The effect of temperature, which was negligible in the Xe particle experiments, has been investigated and controlled in the experiments at KURNS-LINAC. It was found that k_r linearly decreased with increasing beam energy absorbed in the PZT element, whereas the surface temperature remained constant [4]. In terms of that, we propose a dosimeter based on piezoelectric PZT.

EXPERIMENTS IN THE FISCAL YEAR 2022: Although two machine times of LINAC experiment were scheduled for the current year, both experiments were impossible because they coincided with periods of LINAC maintenance and breakdowns.

Although we were unable to conduct electron irradiation experiments using LINAC this year, we conducted experiments using the Pneumatic transport pipe irradiation equipment in KUR to investigate changes in piezoelectricity when PZT samples are irradiated with neutrons. Since this was the first experiment, only one irradiation was conducted on one PZT sample (soft material) to demonstrate proficiency in the experiment. In the future, we would like to continue the experiment by setting multiple irradiation levels and increasing the number of types of irradiated samples.

REANALYSIS OF PAST EXPERIMENTAL DATA: A reanalysis of the data from LINAC experiments up to the previous year was conducted. In earlier analyses of experimental data, we have investigated how the electromechanical coupling coefficient k_r, as an indicator of the piezoelectricity of piezoelectric PZT, changes with electron irradiation. In addition to kr, the mechanical quality factor Q_m was also evaluated in the present study.

As an example of the experimental results, Figure 1 shows the changes of k_r and Q_m versus irradiation dose when piezoelectric PZT, a type of high-temperature soft material, was irradiated by electron beams. As shown in Figure 1, there is an inverse correlation between the increase in the value of the mechanical quality factor and the decrease in the electromechanical coupling coefficient, indicating that the hardening of PZT occurred when only the change in Q_m was examined. This behavior is in contrast to piezoelectric PZT when exposed to high temperatures. In other words, both k_r and Q_m of PZT decrease when exposed to high temperatures, while k_r decreases, but Q_m increases in the case of electron irradiation. These experimental results suggest that the cause of the decrease in k_r due to electron-beam irradiation may be the increase in Q_m; as Q_m increases, the amount of strain against external force decreases, and therefore k_r also decreases. Then, what is the cause of the increase in Q_m, i.e., the "hardening" by electron irradiation? A bold hypothesis is that electron-beam irradiation causes oxygen vacancies in PZT crystals, which in turn causes pinning that prevents the domain walls of the domain structure from moving, but this is still a matter of conjecture. We will need to examine this issue in the future, including how to verify the hypothesis.

Fig. 1. the changes of Kr and Qm versus irradiation dose when piezoelectric PZT, a type of high-temperature soft material, was irradiated by electron beams.

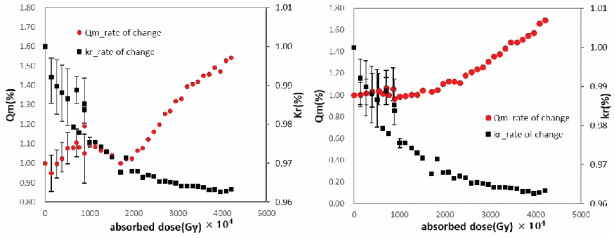

REFERENCES:

[1] M. Kobayashi *et al.,* Jpn. J. Appl. Phys., **52** (2013) 126604.
[2] M. Kobayashi *et al.,* JJpn. J. Appl. Phys., **53** (2014) 066602.
[3] S. Takechi *et al.,* Jpn. J. Appl. Phys., **60** (2021) 038003.
[4] S. Takechi *et al.,* Jpn. J. Appl. Phys., **61** (2022) 128001.
[5] H. Oh'ishi, Master Thesis, Osaka Metropolitan Univ. (2023).

CO4-27 Radiation Induced Demagnetization of Neodymium Magnets

Y. Fuwa, Y. Kuriyama[1], Y. Iwashita[1], K. Takamiya[1], T. Takayanagi

J-PARC Center, Japan Atomic Energy Agency
[1]Institute for Integrated Radiation and Nuclear Science, Kyoto University

INTRODUCTION: Magnets are essential devices in the transport and control of charged particle and neutron beams. Electromagnets have been the primary magnets used in beam experiments so far, but they are being replaced by permanent magnets due to their lower power consumption, compactness, and the fact that they do not require ancillary equipment such as power supplies and cooling water [1-3]. Demagnetization due to radiation is one of the concerns in the use of permanent magnets, but quantitative evaluation of the effect is not sufficient. The importance of this evaluation has increased in recent years due to the increasing intensity of accelerators. Therefore, we are systematically evaluating the effects of demagnetization caused by radiation using the irradiation facilities at the KUR [4].

EXPERIMENTS: In this study, differences in radiation demagnetization effects for neodymium magnets (NdFeB) were evaluated for different dysprosium contents in the material. The irradiated sample were three types of neodymium magnets; N32EZ, N43TS, N52 made by Shin-Etsu Chemical Co., Ltd. These three magnet samples differ in their dysprosium content, with N32EZ, N43TS, and N52 containing more dysprosium in that order, with N52 being a dysprosium-free magnet. The shape of the sample was cylindrical with a thickness of 1 mm and a diameter of 5 mm. The irradiation experiments were performed at KUR Pn-2 port and Tc-Pn. The irradiation time at Pn-2 ranged from 10 seconds to 30 minutes, and at Tc-Pn from 10 minutes to 30 hours. The rate of demagnetization was calculated by comparing the magnitude of magnetization before and after irradiation. The magnitude of each magnetization was evaluated by measuring the magnitude of the induced voltage generated when the magnet sample was rotated near the measuring coil [5].

RESULTS: From Fig. 1, it can be seen that the demagnetization effect of NdFeB magnets with respect to irradiation in Pn-2 is larger as the dysprosium content decreases, and for N52, the magnitude of magnetization decreases to less than 10% of that before irradiation. Similar demagnetization effects have also occurred with irradiation at Tc-Pn (Fig. 2). The thermal neutron flux irradiated at Pn-2 corresponds to 4.9 x 10^{13} n/cm^2 (10 sec.) to 8.8 x 10^{15} n/cm^2 (30 min.), and that at Tc-Pn to 7.6 x 10^{11} n/cm^2 (10 min.) to 1.4 x 10^{14} n/cm^2 (30 hour). For Pn-2 and Tc-Pn, the instantaneous neutron fluxes are 64 times different, (4.9 x 10^{13} n/cm^2/s for Pn-2 and 7.6 x 10^{10} n/cm^2/s for Tc-Pn, respectively), but the effect on demagnetization is not significantly different.

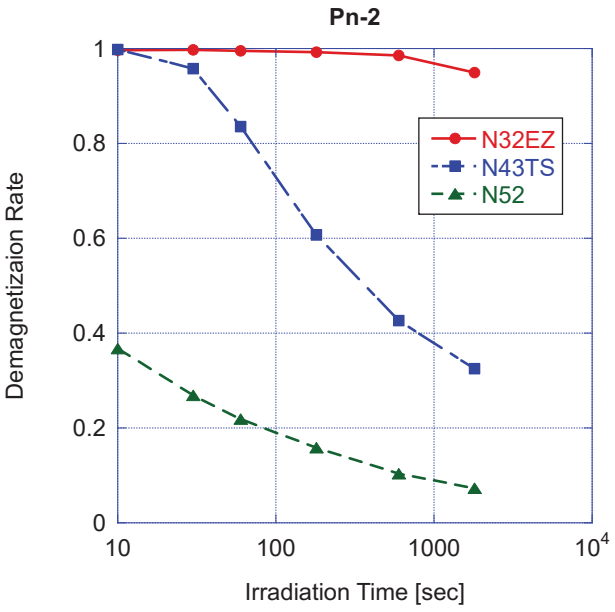

Fig. 1. Measured demagnetization rate of the NdFeB samples irradiated in Pn-2.

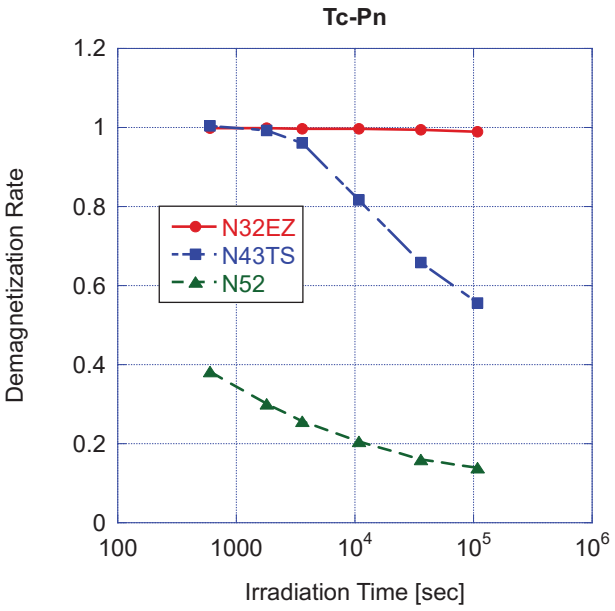

Fig. 2. Measured demagnetization rate of the NdFeB samples irradiated in Tc-Pn.

REFERENCES:

[1] Y. Fuwa *et al.,* Prog of Theor and Exper Physics, **2017(2)** (2017) 023G01.
[2] Y. Kuriyama *et al.,* IEEE Trans. Appl. Supercond., **32(6)** (2022) 4007204.
[3] M. Yamada *et al.,* Prog. Theor. Exp. Phys., **2015(4)** (2015) 043G01 .
[4] Y. Fuwa *et al.,* MT-27 Int. Conf. on Magnet Technology, (2021) TUE-P01-115-05.
[5] Y. Fuwa *et al.,* Proc. of 18th annual meeting of particle accelerator society of Japan, (2021) MOOB07.

CO4-28 Fundamental study of damage on tungsten by heat and particle loading

K. Tokunaga, M. Matsuyama[1], Y. Hatano[1], M. Hasegawa, K. Nakamura and Q. Xu[2]

Research Institute for Applied Mechanics, Kyushu University
[1]Hydrogen Isotope Research Center, University of Toyama
[2]Institute for Integrated Radiation and Nuclear Science, Kyoto University

INTRODUCTION: Refractory metals such as tungsten (W) is potential candidate for the armor of the first wall and the divertor plate of the fusion reactor because of its low erosion yield and good thermal properties. The armor material will be subjected to heavy thermal loads in the steady state or transient mode combined with high energy neutron irradiation that will cause serious material degradation. In addition, high energy runaway electrons would bombard the armor materials along the equatorial plane in fusion device. It is considered that these cause radiation damage and enhance tritium retention. It is of a great importance to clarify phenomena of implantation, retention, diffusion and permeation of tritium (T) on surface of the armor materials of the first wall/blanket and the divertor on fusion device from a viewpoint of precise control of fuel particles, reduction of tritium inventory and safe waste management of materials contaminated with tritium.
In the present works, T exposure experiments have been carried out on W samples which were irradiated by high energy electrons to investigate effects of high energy electrons irradiation on microstructure and tritium retention of W. In this fiscal year, pure W and recrystallized W were irradiated by high energy electron beam. Before and after that, positron annihilation experiment was carried out to identify the radiation defect. In addition, EBSD （Electron Back Scatter Diffraction Patterns） analyses has been carried out on the specimens before and after the electrons irradiation. Tritium exposure experiments have been carried out using a tritium (T) exposure device.

EXPERIMENTS: W samples used were ITER specification W (ALMT-grade) (SR-W) and its recrystallized W (RC-W). The SR-W was fabricated via a powder metallurgical route including cold isostatic pressing, sintering, hot rolling, and heat treating to relieve the residual stresses. Some of the machined SR specimens were subjected to a full recrystallization treatment at 2000 ºC for 1 hr in vacuum. Sizes of the specimens were 10 mm x 10 mm x 1mm (10 mm x 10 mm : ND-TD). The surface of the both samples were polished to be mirrored. High energy electrons irradiation has been carried out using LINAC in Institute for Integrated Radiation and Nuclear Science, Kyoto University. An peak energy of electron irradiated was 8 MeV and DPA was 5.8 x 10^{-3}. Temperature during the irradiation was measured by thermocouples which was contacted with a backside of the W samples. Before and after that, positron annihilation experiment was carried out to identify the radiation defect. In addition, a high energy ion irradiation experiment has stared to carry out. The sample surface was irradiated by 2.5 MeV Fe ions with a flence of 5 x 10^{18} ions/m^2 at RT. T exposure experiments have been carried out using a T exposure device in University of Toyama. Pressure of the T gas was 1.3 kPa and T exposure was kept for 4 h at 100 ºC. T concentration in the gas was about 5 %. After the exposure to T gas, T amount retained in surface layers of the sample was evaluated by imaging plate (IP) measurements and β-ray-induced X-ray spectrometry (BIXS).

RESULTS: Fig.1. shows X-ray spectra observed by BIXS for the non-irradiated SR-W(a), e-irradiated SR-W(b) and ion-irradaited SR-W(c). Temperature of T exposure is 100 ºC. In the case of SR-W(b), WM_{α}, ArK_{α} are detected. These results indicate that T exists the deeper area and the surface of the sample. On the other hand, in the case of SR(c), ArK_{α} are detected. This is attributed by surface retained T. T exposure experiment at 350 ℃ has been carried out.

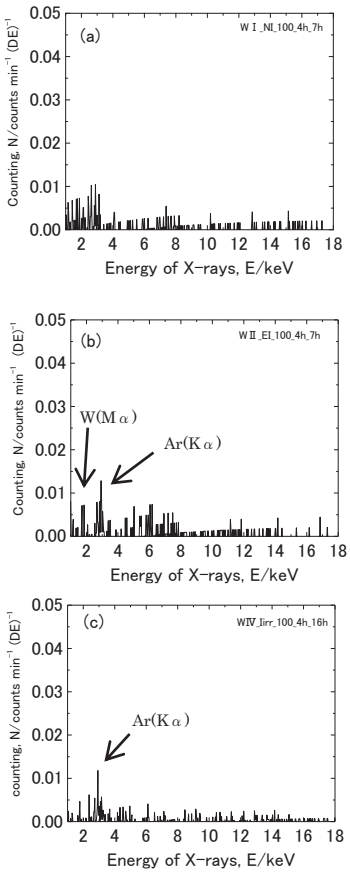

Fig. 1. X-ray spectra for non-irradiated SR-W(a), e-irradiatyed SR-W(b) and ion irradiated SR-W(c).

CO4-29 Vacancy Migration Energy in CrFeNi Medium-Entropy Alloy

H. Araki, K. Sugita, M. Mizuno, A. Yabuuchi[1] and A. Kinomura[1]
Graduate School of Engineering, Osaka University
[1]*Institute for Integrated Radiation and Nuclear Science, Kyoto University*

INTRODUCTION: Tsai *et al*. [1] originally proposed the concept of sluggish diffusion, based on a positive correlation between the activation energies for atomic diffusion, which are normalized by the melting temperature, T_m , and the number of constituent elements in the CrMnFeCoNi high-entropy alloy(HEA) and its subsystems. However, the reason for the sluggishness of diffusion is not quite clear.

In the CrMnFeCoNi HEA and its subsystems at high temperatures, atomic diffusion is expected to proceed via a vacancy mechanism because they are substitutional solid solutions. Therefore, vacancy formation and migration energies in the CrMnFeCoNi HEA and its subsystems are important indexes for understanding the sluggish diffusion. In this work we have evaluated the vacancy migration energy in CrFeNi medium-entropy alloy by observing the vacancy migration and annihilation behavior during an annealing process after electron irradiation, with the use of the positron lifetime spectroscopy.

EXPERIMENTS: An arc-melted ingot of CrFeNi alloy was homogenized at 1373K for 24 h under argon atmosphere, and cut into 10 mm × 10 mm × 0.5 mm plates. The plates were polished and then sealed in silica tubes. Solution heat treatment was carried out for 1 h at 1373 K and the samples were quenched in water. Their X-ray diffraction analysis shows that all the samples are composed of single phase with a fcc structure. Then, the samples were irradiated in water with 8 MeV electrons at a fluence of approximately, 1×10^{22} e^{-} m^{-2} below 358 K using the electron linear accelerator at the Institute for Integrated Radiation and Nuclear Science, Kyoto University. The irradiated samples were isochronally annealed in a temperature range from 373 to 673 K. The temperature step during the isochronal annealing was 25 K and the duration of exposure to each temperature was 1 h.

The positron lifetime measurements were made at 297–299 K using a fast-fast timing coincidence system with a time resolution(FWHM) of 180–183 ps.

RESULTS: Before the electron irradiation the positron lifetime spectrum for the solution-treated alloys was represented by only one component of 108 ps, which is approximately equal to the values calculated for the defect-free constituent pure metals. This indicates that positrons annihilate in the bulk for the solution-treated alloy sample. After electron irradiation, the mean positron lifetime was increased to 136 ps. The analysis of positron lifetime spectra for the as-irradiated sample shows that many positrons are trapped and annihilate in the monovacancies introduced by electron irradiation, because the lifetime component, τ_2 , of trapped positrons was 180 ps, which is in agreement with the experimental values for monovacancies in the constituent pure metals. Assming that the specific trapping rate of monovacancies, μ_v , is 10^{15} s^{-1}, the vacancy concentration in the as-irradiated sample is of the order of a few atomic parts per million.

Fig.1 shows the change in the vacancy concentration during the isochronal annealing of the irradiated sample, which was evaluated on the basis of the two- or three-component analyses for the positron lifetime spectra. In the temperature range where dislocations and monovacancies are expected to coexist, the positron lifetime spectra were analyzed on the assumption that the positron lifetime component of dislocation is 150 ps. As shown in Fig.1, the vacancy concentration decreases with annealing temperature, because the vacancies introduced by electron irradiation gradually disappear as the vacancies become mobile during the isochronal annealing. The decrease in the vacancy concentration was theoretically analyzed on the basis of Dryzek *et al*.'s model for isothermal annealing [2] .

Assuming that the vacancy migration energy is constant over the whole temperature range, there remains a few discrepancies between the theoretical fitting model and the experimental data, as shown in Fig.1. The positron lifetime measurements indicate that dislocation loop components are detected in addition to vacancies at high temperatures, suggesting that the vacancy migration process is easily influenced by the presence of dislocations. Therefore, we assumed two-component vacancy migration energies (H_m^L , H_m^H) and optimized their values to fit the experimental data. The value of H_m^L obtained in the low temperature range is 0.79 eV, which is nearly equal to 0.77 eV of effective vacancy migration energy obtained in an analysis of the void-denuded zone widths formed in a $Fe_{55.8}Cr_{16.1}Ni_{28.8}$ alloy under neutron and electron irradiation[3].

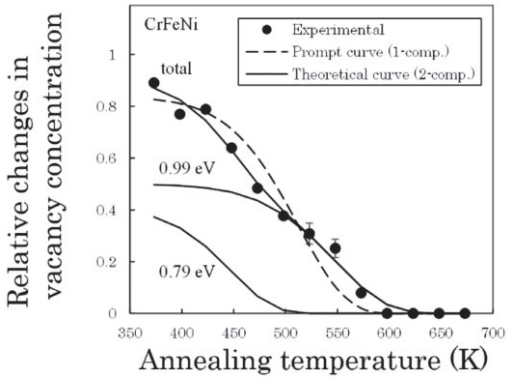

Fig. 1. The relative changes in vacancy concentration ob-tained from experiments and theoretical calculations.

REFERENCES:

[1] K. Y. Tsai *et al.,* Acta Mater., **61** (2013) 4887.
[2] J. Dryzek *et al.,* Ma-ter. Lett., **21** (1994) 209.
[3] Y. Sekino and N. Sakaguchi, Mater. Trans., **60** (2019) 678.

CO4-30 A study on destruction of cesium aluminosilicate compounds by gamma irradiation (4)

H. Ohashi, R. Tawatari, T. Saito[1]

Faculty of Symbiotic Systems Science, Fukushima University

[1]Institute for Integrated Radiation and Nuclear Science, Kyoto University

INTRODUCTION: Pollucite which is one of cesium aluminosilicate compounds have attracted attention as a fi-nal storage material of ^{134}Cs and ^{137}Cs. Pollucite is easily synthesized by hydrothermal method in low temperature below 300°C [1]. Pollucite has various properties that fa-vor the immobilization of Cs ions.

However, the damage to the aluminosilicate framework by radiation decay is concerned because it contains ^{134}Cs and ^{137}Cs. It has been reported that the effect of β-ray emis-sion and nuclide conversion by β-decay of ^{137}Cs on alumi-nosilicate framework is minor [2, 3]. On the other hand, there are few reports of effects by gamma rays on pollucite framework. Therefore, we examined the effect of gamma radiation on the aluminosilicate framework of Pollucite. In this report, we have studied on cesium leakage from pol-lucite and various aluminosilicate.

EXPERIMENTS: Sodium aluminate, sodium metasilicate and cesium chloride were dissolved in sodium hydroxide solution. The solution was placed in a Teflon inner cylinder pressure container. Pollucite was synthesized by hydrothermal method, holding the container at 180°C for 12 hours. The resulting precipitate was washed by distilled water. Thereafter, each solid was collected by filtration and dried at 110°C for 12 hours or more. Adsorption experi-ments were performed using mordenite, bentonite and Ze-olite 13X, Zeolite 4A. Each adsorbent was added to 0.1 M cesium chloride solution and stirred for 24 hours. The amount of cesium absorbed was estimated by atomic ab-sorption spectrophotometry.

The powder samples were characterized by XRD, and gamma-irradiated with 87.9 kGy by ^{60}Co source. The leaching test by PCT-A method [4] was carried out to eval-uate the change of Cs retention performance by framework damage. Concentration of cesium in solution leached was estimated by atomic absorption spectrophotometry. Leach-ing rate was calculated by equation (1).

$$\boldsymbol{LR}\ (\%) = \frac{\boldsymbol{C_{Cs}V \times 10^{-3}}}{\boldsymbol{mf_{Cs}}} \times \boldsymbol{100} \qquad (\boldsymbol{1})$$

Where C_{Cs} [mg L^{-1}] was the concentration of Cs in the solution, m was the weight of samples, f_{Cs} was the weight ratio of the Cs in the sample before leaching, V [L] was the volume of the leaching liquid.

RESULTS: It was confirmed from the result of atomic absorption spectrometry that cesium was adsorbed on the adsorbent. Figure 1 shows the XRD pattern of samples. The sample synthesized for 12 hours was confirmed to be pollucite.

Table 1. shows the results of leaching tests performed with various aluminosilicates. As a result of the table, it was turned out that pollucite had a lower leaching rate than other cesium-containing aluminosilicates.

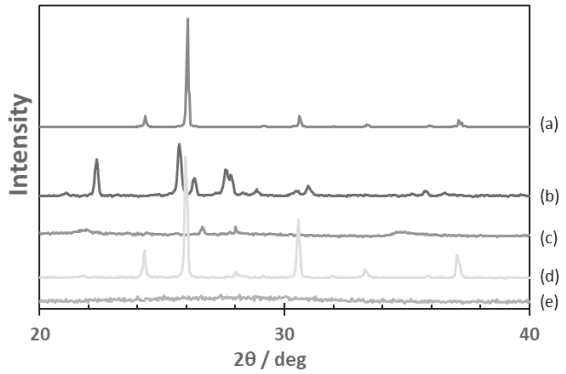

Fig. 1. XRD patterns of samples. (a)Pollucite-std, (b)Cs_{ad} Mor-denite, (c)Cs_{ad} Bentnite, (d)Pollucite, (e)Amorphous.

Table 1. Results for PCT-A-like leaching test.

Sample	T / °C	t / hr	C_{Cs} / mg L^{-1}	Leaching rate /%
Cs_{ad} MOR	**90**	**168**	**144**	**0.620**
Cs_{ad} Bentnite	**90**	**168**	**267**	**1.50**
Cs_{ad} Zeolite13X	**90**	**168**	**245**	**1.03**
Cs_{ad} Zeolite4A	**90**	**168**	**368**	**2.00**
Pollucite	**90**	**168**	**13**	**0.0425**
Amorphous	**90**	**168**	**989**	**92.3**

REFERENCES:

[1] Y. Yokomori *et al.*, Sci. Rep., **4** (2014), 4195.
[2] J. Fortner *et al.*, Argonne National Laboratory, Argonne, Illinois **60439** (2001).
[3] N. J. Hess *et al.*, J. Nucl. Mater., **281** (2000), 22-33.
[4] ASTM C 1285-02 (2008).
[5] Z. Jing *et al.*, J. Hazard. Mater., **306** (2016), 220-229.

CO4-31 Radiotolerance analysis of *Deinococcus sp.* strain AKn-1 isolated from the coast of Akina bay in Amami-Oshima Island

H. Ohashi, K. Matsubara[1], T. Saito[2] and T. Sakaguchi[1]

Faculty of Symbiotic Systems Science, Fukushima University

[1]Department of Life Science, Prefectural University of Hiroshima

[2]Institute for Integrated Radiation and Nuclear Science, Kyoto University

INTRODUCTION: Since discovery of *Deinococcus spp.*, its microorganisms have been well known for their resistance to strong radiation, and have been found in many environments such as deserts, muddy soils, and aerial environments. We have studied properties of *Deinococcus spp*. Recently we have isolated the AKG-1 strain, which produces a red pigment from slime on the body surface of the yellowbarred red rockfish. Its strain was classified in *Deinococcus sp.* and had resistant to hydrogen peroxide and ultraviolet rays. The results suggested that the *Deinococcus spp*. would have a wide distribution of in the marine environment.

In this study, we examined the isolation and culture of *Deinococcus* microorganisms from samples taken from the sandy beach in Amami-Oshima Island with strong ultraviolet rays. Furthermore, the gamma ray resistance of the obtained UV-resistant isolate AKn-1 strain was investigated.

EXPERIMENTS: The sand and seawater along the coast of Amami-Oshima Island, which is assumed to be a harsh growing condition due to the high exposure to ultraviolet rays, was collected during the daytime on a sunny day and used as an isolated sample of the target microorganism. After that, normal culture and isolation operation were performed.

The strain obtained above and the *E. coli* JM109 strain were made into a suspension solution, and each suspension solution was irradiated with ^{60}Co gamma ray at the Institute for Integrated Radiation and Nuclear Science, Kyoto University.

The irradiated samples were diluted with YMs medium, inoculated and cultured on a plate. Then, Colony Forming Units (CFU) were counted. The surviving fraction was estimated from the CFU ratio of non-irradiated and irradiated samples.

RESULTS: As a result of isolating and culturing, we succeeded in obtaining an isolated strain (named "AKn-1 strain") resistant to selenate and ultraviolet rays from the sandy beach of Akina Bay, Tatsugō, Kagoshima Prefecture, Japan. The strain was cocci or diplococci with a size of 1-2 μm and had a non-migrating cell morphology. In addition, it was Gram-positive and closely resembled *Deinococcus sp.* AKG-1 strain.

Fig.1. shows a plot of the surviving fraction of cells as measured by the number of colonies formed by the surviving cells relative to the control. Both *Deinococcus sp.* AKG-1 and *Deinococcus sp.* AKn-1 strains were found to be radiotolerant compared to *E. coli* JM109 strain.

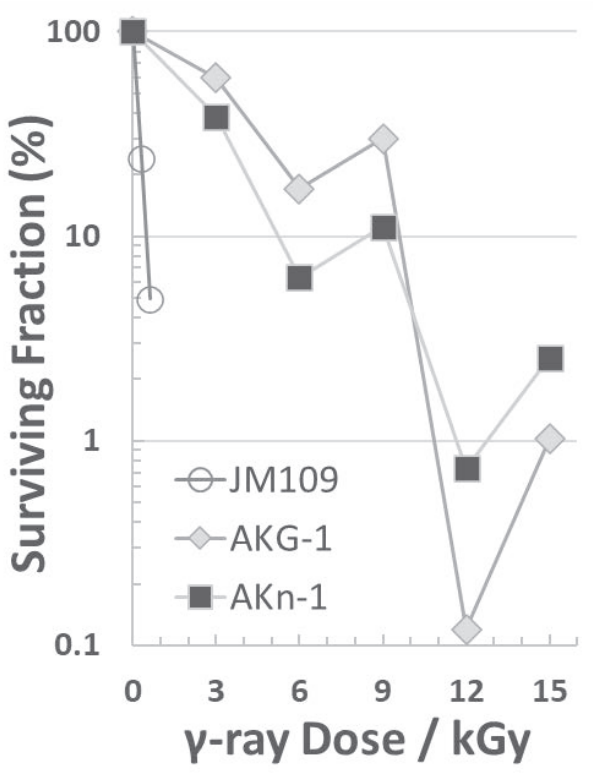

Fig.1. Surviving fraction of cells as measured by the number of colonies formed by the surviving cells relative to the control. ○: *E. coli* JM109 strain, ◇: *Deinococcus sp.* AKG-1 strain, and ■: *Deinococcus sp.* AKn-1 strain.

CO4-32 TDPAC Measurement of ^{111}Cd(←^{111}In) in Ultrafine Bubble Water

M. Tanigaki, Y. Ohkubo, A. Taniguchi, Y. Ueda[1], Y. Tokuda[2]

Institute for Integrated Radiation and Nuclear Science, Kyoto University
[1]Research Institute for Sustainable Humanosphere, Kyoto University
[2]Department of Education, Shiga University

INTRODUCTION: Ultrafine bubbles, the gaseous cavities with diameters less than one micrometer, have recently attracted much attention because of their multi-functionalities [1]. Fundamental studies on such multi-functionalities of ultrafine bubbles are not well extended because they are smaller than the wavelength of radiant rays. The time differential perturbed angular correlation (TDPAC) of ^{111}Cd(¬ ^{111}In) in the aqueous solution with ultrafine bubbles is performed for the study of the interface of ultrafine bubbles, which should be one of the essential origins of its multi-functionality.

EXPERIMENTS: Typical four-counter TDPAC measurements were performed for the 171-245 keV cascade in ^{111}Cd(¬ ^{111}In) in aqueous solutions of pH = 7~8, 10~10.5 with/without Oxygen-ultrafine bubbles. The average diameter and the density of the ultrafine bubbles in each sample were measured by Archimedes to be 115 nm and 2.45 ×10^6/mL, respectively. ^{111}In was obtained from Nihon Medi-Physics as the aqueous solution of $^{111}InCl_3$ at a pH of approximately 2. This ^{111}In solution was added to each aqueous solution sample. The pH control was performed by adding Na_2CO_3 for better pH control around pH = 7 instead of NaOH in the previous study [2]. The angular correlation term $A_{22}G_{22}(t)$ is given by the following equation,

$$A_{22}G_{22}(t) = \frac{2\left(N(180°,t)-N(90°,t)\right)}{N(180°,t)+2N(90°,t)},$$

where $N(90°, t)$ and $N(180°, t)$ are the counting numbers of the 171-245 keV γ-γ cascade at 90 and 180 degrees, respectively. The time-dependent term $G_{22}(t)$ for each sample was obtained by normalizing obtained $A_{22}G_{22}(t)$ by the asymmetry parameter of 171-245 keV cascade in ^{111}Cd, $A_{22} = -0.18$.

RESULTS AND DISCUSSIONS:
Observed $G_{22}(t)$ are shown in Fig. 1. and 2. Those were similar to the cases of pH = 7.4 and 13.4 reported by Demille [3]. The initial drops at 15 to 20 ns in $G_{22}(t)$ were more significant in Oxygen-ultrafine bubble water than those in pure water regardless of their pH. This difference may be caused by the influence of the ultrafine bubbles to the formation of hydrated ions of In. More studies, such as the detailed pH dependence, are underway.

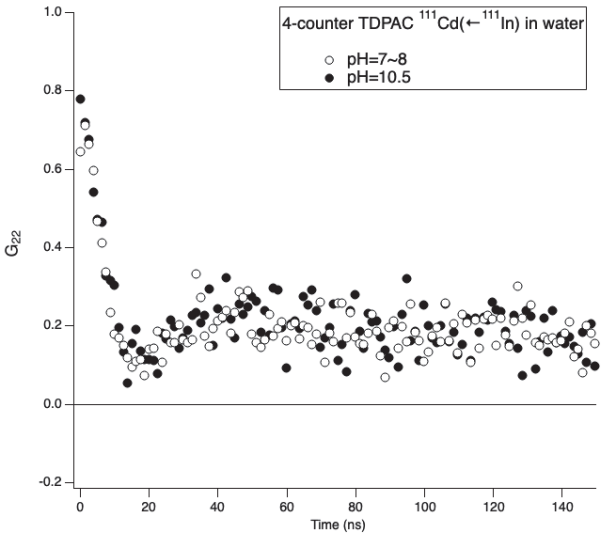

Fig. 1. TDPAC spectra of ^{111}Cd(¬ ^{111}In) in pure water at pH = 10~10.5 and 7~8.

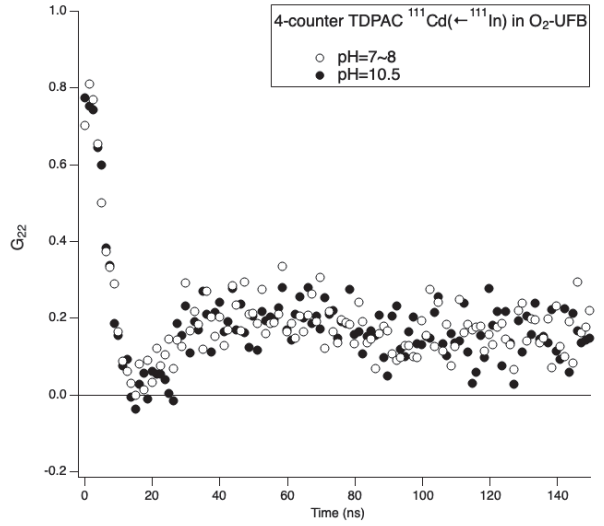

Fig. 2. TDPAC spectra of ^{111}Cd(¬ ^{111}In) in ultrafine bubble water and pure water at pH = 10~10.5.

The present work is supported by JSPS KAKENHI Grant Numbers 18K03948 and 21K03854.

REFERENCES:
[1] E. G. Denis, The fine bubble break-through. https://www.iso.org/news/2014/05/Ref1844.html.
[2] M.Tanigaki *et al.,* KURNS Progress Report 2021, (2022) 124.
[3] G. R. Demille *et al.,* Chemical Physics Letters, **44** (1976) 164-168.

CO4-33 Low Energy Positron Annihilation Lifetime Spectroscopy of Chromium Oxynytride Epitaxial Films on Magnesium oxide crystalline substrates

M. Kitaura, S. Watanabe[2], T. Sugai[3], T. Suzuki[3], J. Kinomura[4]

Faculty of Science, Yamagata University
[1]Institute of Innovative Research, Tokyo Institute of Technology
[2]Graduate school of Engineering, Nagaoka University of Technology
[3]Institute for Integrated Radiation and Nuclear Science, Kyoto University

INTRODUCTION: Epitaxially grown chromium oxide films on magnesium oxide crystal substrates have the NaCl type (B1) structure, same as chromium nitride films. Rutherford backscattering spectroscopy (RBS) measurement revealed that the compositions of chromium oxide epitaxial films is Cr_2O_3, similar to corundum type [1,2]. In order to obtain Cr_2O_3 with the B1 type structure, vacancies
have to be introduced at the chromium site. However, there is no evidence concerning the introduction of such chromium vacancies by oxygen replacement in chromium nitride. Vacancy-induced B1 structures have also been observed for other 3d transition metal monoxides such as VO and TiO. Positron annihilation lifetime spectroscopy (PALS) has been used to investigate the nature of vacancy-type defects in solids [3,4]. In the present study, PALS spectra of chromium oxynitride epitaxial films with different oxygen contents were measured.

EXPERIMENTS: Samples of epitaxially grown chromium oxynitride files on magnesium substrates were prepared by the pulse laser deposition (PLD). The average thickness of samples was 300 nm. PALS measurements were performed using slow positron beam from Kyoto University Research Reactor (KUR). The incident energy of the slow positron beam was adjusted by the Doppler broadening measurements of positron annihilation with valence electrons in chromium oxynitride epitaxial films. To obtain PALS spectra, positron annihilation gamma-rays were detected until the number of evens for it reaches 100000 counts. The lifetime was analyzed using the software LT9 [5].

RESULTS: PALS spectra of chromium oxynitride epitaxial films were reproduced by two exponential decay functions. The first component with a shorter lifetime was dominant. The intensity of the second component with a long lifetime was only a few percent. The variation of the lifetime of the first component for chromium oxynitride epitaxial films is shown in Fig. 1 for several oxygen content x. The lifetime was apparently increased with x. This fact indicates that the positron annihilation site changes with x. As mentioned above, the replacement of

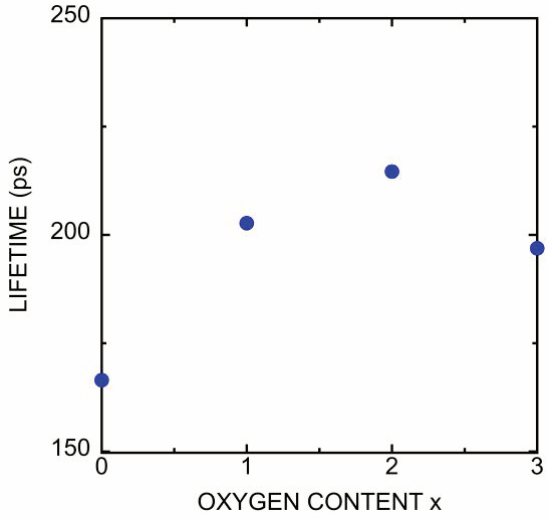

Fig.1. Variation of the lifetime of the first component for chromium oxynitride epitaxial films.

nitrogen by oxygen is expected to introduce chromium vacancies in chromium oxynitride epitaxial films. The longer lifetime of the first component suggests that most of positrons annihilation at chromium vacancy sites in chromium oxynitride epitaxial films of x=1. The lifetime was slightly increased at x=2. Divacancy or trivacancy may be predominantly formed in $1<x<2$, because the lifetimes of them are slightly larger than that of monovacancy. The lifetime was slightly shortened at x=3. In refs. [1,2], stacking faults due to corundum Cr_2O_3 were increased with x. Vacancy complexes in the B1 type structure will partially participate the formation of the stacking fault, in which they are changed into the interstitial open space. This process competes with the formation of vacancy complexes in the B1 type structure. Consequently, vacancy complexes are suppressed with increasing x, and thus the lifetime is decreased at x=3.

REFERENCES:

[1] K. Suzuki *et al.*, Thin Solid Films **625** (2017) 111-114.
[2] K. Suzuki *et al.*, APL Mater. **3** (2015) 096105/1-6.
[3] K. Fujimori *et al.*, Appl. Phys. Express, **13** (2020) 085505/1-4.
[4] M. Kitaura *et al.*, Opt. Mater.: X **14** (2022) 100156/1-7.
[5] J. Kansy, Nucl. Instrum. Methods Phys. Res. Sect. A, **375** (1996) 235-244.

CO4-34 Influence of Hydrogen Isotopes on Growth of Vacancy Clusters in Tungsten-Based Materials

Y. Hatano, M. Matsumoto[1], T. Asano[1], M. Nishimura[1], T. Takahashi[2], N. Abe[2] and A. Kinomura[2]

Hydrogen Isotope Research Center, University of Toyama
[1]Guraduate School of Science and Engineering, University of Toyama
[2]Institute for Integrated Radiation and Nuclear Science, Kyoto University

INTRODUCTION: As a plasma-facing material of a future fusion reactor, tungsten (W) will be exposed to intense flux of fuel particles, deuterium (D) and tritium (T), and that of products of fusion reactions, helium and 14 MeV neutrons. Irradiation of 14 MeV neutrons induces displacement damages in a W lattice. The authors have found that neutron irradiation drastically increases fuel retention in W due to trapping effects by vacancies and vacancy clusters [1]. Understanding of vacancy formation and clustering is necessary for accurate evaluation of T inventory in a vacuum vessel of a reactor.

In previous studies [1-3], W samples were irradiated with neutrons or heavy ions first, and then hydrogen isotope was introduced by plasma or gas exposure. However, in real fusion conditions, the radiation-induced defects are accumulated under exposure to hydrogen isotope plasma. Hence, the influence of hydrogen isotopes on the development of damaged structure must be understood.

The objective of this study is to investigate vacancy clustering in W under the presence of hydrogen isotopes and to construct a kinetic model of clustering. To reach this goal, W samples with monovacancies are prepared by electron beam irradiation. Then, the irradiated samples are heated with and without hydrogen isotopes, and the difference in size distributions of vacancy clusters is examined using positron annihilation spectroscopy.

EXPERIMENTS: Samples were disks of W with 6 mm diameter and 0.5 mm thickness prepared from a rod provided by A. L. M. T. Co., Japan. After surface polishing to mirror-like finish, the samples were annealed in vacuum ($<10^{-5}$ Pa) at 1273 K for 1 h to relieve stress potentially induced during machining and polishing.

The electron linear accelerator at Institute for Integrated Radiation and Nuclear Science, Kyoto University, was used for electron beam irradiation. Eight samples were stacked in two layers of four samples, as shown in Fig. 1. The stacked samples were wrapped with aluminum (Al) foil and sealed using Al tape. Then, the samples were put into an Al chamber and irradiated with 8 MeV electrons for 77 h to 5×10^{-3} dpa. During irradiation, the samples were cooled by water circulating in the chamber over the Al tape. The temperature of the samples was measured using a thermocouple insulated with a polyimide film and attached on the Al tape. However, signal was lost during the irradiation probably due to damaging in the polyimide film. After the irradiation, the positron lifetime was measured using 1 MBq ^{22}Na source at Institute for Materials Research, Tohoku University. A total of 9×10^6 coincidence events were collected for each measurement, and the lifetime spectrum was analyzed using PALSfit software package [4].

RESULTS: Positron lifetime spectra for non-irradiated and electron-irradiated samples are given in Fig. 2. Clear increase in positron lifetime was observed after electron irradiation. The positron lifetime in the non-irradiated samples was ~130 ps. The lifetime spectra for the irradiated samples were reproduced by assuming presence of two components: ~140 ps and ~360 ps. The shorter component showed formation of monovacancies. The longer component indicated that vacancy clusters were formed during irradiation though the samples were cooled by flowing water. D will be introduced into the samples by plasma exposure and cluster growth will be investigated in the next year.

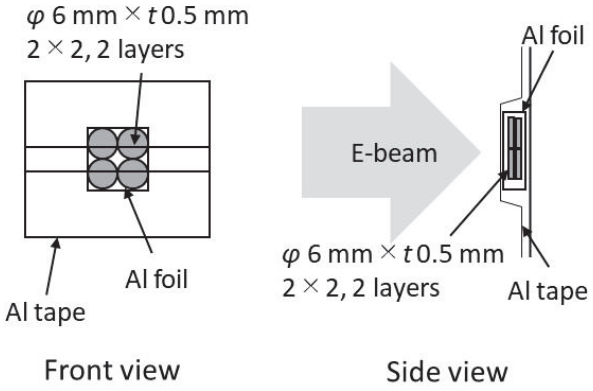

Fig. 1. Arrangements of W samples during electron irradiation.

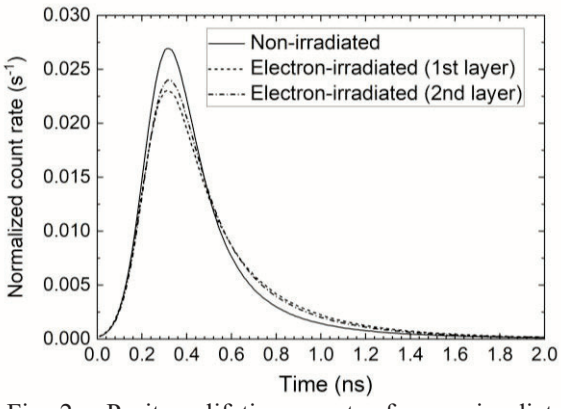

Fig. 2. Positron lifetime spectra for non-irradiated and electron-irradiated W.

REFERENCES:

[1] T. Toyama *et al.,* J. Nucl. Mater., **499** (2018) 464-470.
[2] M. Yajima *et al.*, Phys. Scr., **96** (2021) 124042.
[3] J. Wang *et al.*, J. Nucl. Mater., **559** (2022) 153449.
[4] J. V. Olsen *et al.*, Phys. Stat. Sol. C., **4** (2007) 4004-4006.

CO4-35 Magnetic Measurememts of Irons in Soda-lime Glass by Mössbauer Spectroscopy

K. Okada and Y. Kobayashi[1]
SPring-8/JASRI
[1]Institute for Integrated Radiation and Nuclear Science, Kyoto University

INTRODUCTION and AIM: Glass is used in many applications in our every-day lives and has exciting new applications related to the energy. Soda-lime glass is made of mainly silica (SiO_2) and additive many other materials, such as magnesium, sodium, calcium, aluminum, iron, sulfur, and so on. Our sample glass composition, in percent by weight (wt%), was 72.25 SiO_2, 1.75 Al_2O_3, 4.00 MgO, 8.00 CaO, 14.00 Na_2O as basic components, and 0.015-5 iron in terms of Fe_2O_3 as coloring and functional components. Iron contaminants of less than 0.0005-0.01 wt% are from raw materials, and irons up to 1.5-5 wt% are from injection. The iron oxides in a glass composition are thought to be present in forms of Fe^{3+} and Fe^{2+}. The control parameters for irons are two: (1) the total iron mass weight percent in terms of Fe_2O_3, and (2) the number ratio of Fe^{2+} to total iron ions ($\Sigma_n Fe^{2+}/(\Sigma_n Fe^{2+}+\Sigma_n Fe^{3+})$). The Fe^{3+} component adds a light yellow tint to the glass and absorption in the ultraviolet and visible band, while the Fe^{2+} component adds a blue tint to the glass and absorption in the near-infrared band (1 μm). The transmission from ultraviolet to infrared in glass cannot be explained by simple Fe^{2+} and Fe^{3+} structures. Then, to reveal the exact local structures of irons (Fe^{2+} and Fe^{3+}) is necessary. Many scientists proposed many new theories and local structures [1-4], but they did not resolve it completely.

We have prepared glass samples using the Mössbauer isotope ^{57}Fe (natural abundance is about 2.119 %). The chemical composition of iron oxide in the ^{57}Fe enrichment glass samples was from 0.015 to 5 wt%, and the $\Sigma_n Fe^{2+}/(\Sigma_n Fe^{2+}+\Sigma_n Fe^{3+})$ was from 0 to 0.6. We have investigated these samples by nuclear resonant inelastic scattering and X-ray Absorption Fine Structure methods at synchrotron radiation to reveal the local atomic structure around and neighboring iron atoms in sub-nanometer region[5]. And then we have investigated same samples by the Electron Spin Resonance and the Superconducting Quantum Interference Device measurements to reveal the magnetic property in glass. From these results, the capability of complex magnetic fields according to the only Fe^{3+} atoms or both of Fe^{3+} and Fe^{2+} atoms was suggested. By Mössbauer experiments, we can get magnetic moments and magnetic states at various temperatures. Then we proposed the Mössbauer measurements to reveal the magnetic property and the magnetic state from Fe^{3+} and Fe^{2+} atoms independently.

EXPERIMENTS: The measurements were performed using conventional Mössbauer spectrometer. The specimens for Mössbauer measurements were tuned to 10 mm-phi pellet from the ^{57}Fe enriched glass powders. We investigated one new sample including irons of 0.1 wt% with 0.6 $\Sigma_n Fe^{2+}/(\Sigma_n Fe^{2+}+\Sigma_n Fe^{3+})$ at room temperature.

RESULTS and DISCUSSION: The data of samples including iron of 0.1 wt% with 0.2 and 0.6 $\Sigma_n Fe^{2+}/(\Sigma_n Fe^{2+}+\Sigma_n Fe^{3+})$ were showed in Fig. 1. As shown in Fig. 1, there was the difference of continuous wide components between the $Fe^{2+}/(\Sigma_n Fe^{2+}+\Sigma_n Fe^{3+})$, and these structures indicated the local magnetization around iron atoms. The Fe^{3+} components with large internal magnetic field have been detected. And the results from various iron oxide content glass indicated the Fe^{3+} and Fe^{2+} atoms were in glass as separate structures.

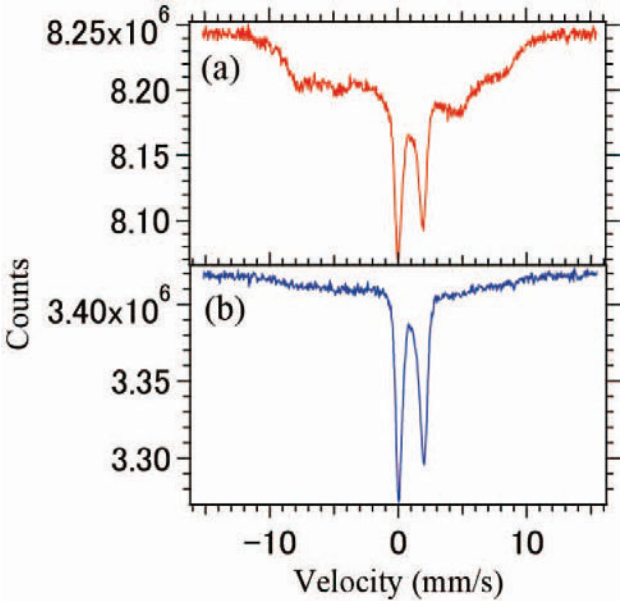

Fig. 1. Mössbauer spectra of soda-lime glass with 0.1 wt% iron oxide comprising. The **$Fe^{2+}/(\Sigma_n Fe^{2+}+\Sigma_n Fe^{3+})$** was (a) 0.2, and (b) 0.6. The measurements were performed at room temperature.

REFERENCES:

[1] C. Ruessel *et al.*, Phys. Chem. Glasses, **47** (2006) 563.
[2] T. Uchino *et al.,* J. Non-Cryst. Solids, **261**(2000) 72.
[3] F. Farges *et al.*, Physica Scripta, **T115** (2005) 957.
[4] C. Russel, Glastech. Ber., **66** (1993) 68.
[5] K. Okada *et al.*, X-ray Spectrometry, **47** (2018) 359-371.

CO4-36 Gamma-ray energy separation by shielding material for 1F debris destribution estimation

Y. Okuno[1,2] and N. Sato[2]

[1]RIKEN
[2]*Institute for Integrated Radiation and Nuclear Science, Kyoto University*

INTRODUCTION:

At TEPCO's Fukushima Daiichi nuclear power plant(1F), fuel debris removal began in December 2021, and full-scale decommissioning will take place over the next several decades. However, the location of debris has not been sufficiently identified, and sensors for debris exploration is required. The gamma rays emitted from fuel debris and the others are expected to originate from Eu-154, and Cs-134, Ba-137, Co-60, and Pr-144, respectively. Since debris-specific gamma rays are predominantly seen in the energy region above 1 MeV, designing a detector that can roughly separate the energies above and below 1 MeV will enable us to determine the rough distribution of debris. Also, since Co-60 gamma rays present the noise in the Eu-154 signal above 1 MeV, auxiliary neutron flux measurements would improve the accuracy of the fuel debris location characteristics. We envision the use of solar cell dosimeters as dosimeters for debris exploration[1]. However, it is difficult for a single element to discriminate between radiation types and energies. Therefore, in this study, a new energy-separation method is proposed that uses a radiation low-cut filter that preferentially attenuates low-energy gamma rays below 1 MeV by shielding. Using shielding materials of two or more different elements, it is assumed to analyze debris-derived gamma rays from the difference in dosimeter signals resulting from the difference in the energy dependence of the attenuation coefficients of photoelectric and Compton effects.

****

RESULTS:

As shown in Fig.1, 18.1 mm beryllium and 2 mm lead were used as low-cut filters, and the filter characteristics above and below 1 MeV were obtained using Cs-137 and Co-60 gamma sources. The current signal of the solar cell dosimeter using amorphous silicon solar cells with Pb shield attenuated just the gamma-ray from Cs-137 such as below 1 MeV gamma rays. Solar cells also can detect neutrons in the case of charged particle conversion film such as boron placed on the surface. The signal of with and without the conversion film installed InGaP solar cell under the condition of neutron irradiation using the small accelerator neutron source RANS[2]. The results show that RANS neutrons can be efficiently detected by the conversion film. Therefore, there is a possibility that information on fuel debris can be identified by scanning measurement of gamma-ray-energy-separation and gamma-ray-neutron-separation with multiple solar cell type dosimeter adjusted the structure of shield and conversion film installed at the same position, such as on a robot arm.

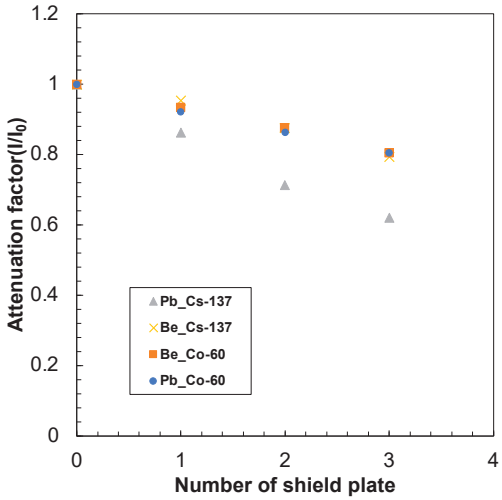

Fig. 1. Signal attenuation factor of solar cell dosimeters due to the installation of shielding material.

****

EXPERIMENTS:

The irradiation sample was amorphous silicon solar cell. Irradiation source was ^{137}Cs gamma-ray at Tokyo Metropolitan Industrial Technology Research Institute and ^{60}Co at Institute for Integrated Radiation and Nuclear Science. The sample was set at under the irradiation environment and was connected with electrometer (iDC13, Taieidenki co.) at the measurement room by using BNC cable.

****

REFERENCES:

[1] Y. Okuno *et.al,* ACS Appl. Electron. Mater., **4** (2022) 3411-3420.
[2] Y. Otake, Reviews of Accelerator-Science and Technology, **8** (2015) 181-207.

CO4-37 Study on activation of neutron optical elements in a new research reactor

H. Fujioka, K. Mishima[1], Y. Yamagata[2], and K. Takamiya[3]

Department of Physics, Tokyo Institute of Technology
[1]Institute of Material Structure Science, KEK
[2] RIKEN Center for Advanced Photonics, RIKEN
[3]Institute for Integrated Radiation and Nuclear Science, Kyoto University

INTRODUCTION: To extract neutron beams efficiently from a research reactor, it is important to increase the solid angle of extraction by using a focusing optical system, as well as to improve the performance of the cold neutron source itself. This is achieved by inserting a neutron guide tube with rotating parabolic or ellipsoidal surface as close as possible to the cold neutron source. In this case, the neutron mirror is placed in a high radiation environment near the reactor core, and the radiation resistance and activation evaluation are necessary. In addition, diamond nanoparticles (DNP) can change the direction of flight of neutrons that are not fully reflected by the mirror to the beam extraction direction by neutron scattering, and are expected to increase the extraction amount of neutrons, especially long-wavelength neutrons. In this study, we irradiate metal materials used as substrates for neutron reflectors at KUR, and investigate the activation analysis and physical damage of the substrate surface. Since physical damage caused by radiation may increase the surface roughness, we compare the surface roughness before and after irradiation. We also perform activation analysis on DNP in the same way.

EXPERIMENTS: Two DNPs and two mirrors were irradiated in the KUR nuclear reactor to investigate radiations due to impurities in them.

For DNP samples, uDiamond® Molto Nuevo (DNP#01) from Carbodeon and RT-DND-B (DNP#02) from Ray Techniques were used. Each DNP power of 0.1 g was sealed in a plastic case, inserted into the radiation field through the KUR pneumatic transport tube Pn-2, and irradiated for 12 seconds. The reactor power was 5 MW and the neutron dose was estimated to be 2.6×10^{13} n/cm^2/s. Gamma-ray spectra were obtained by a HPGe detector after irradiation, and activation analysis was performed.

For neutron mirrors, two pieces of aluminum mirror coated with electroless NiP plating (50 μm) (10 mm x 15 mm x 2 mmt) were used for the irradiation experiment. These samples were irradiated through Pn-2 port with radiation time of 6 and 360 seconds. As well as DNP, the residual Gamma-ray spectra was measured by HPGe. In addition, to check whether the surface roughness was not degraded by irradiation, a replica of the NiP was taken on a sheet and the surface condition was observed.

RESULTS: For DNPs, the post-irradiation doses were estimated to be 75 kBq for DNP#01 and 280 kBq for DNP#02. Impurities such as Na, Cl, Mg, and Ti were detected at several hundred to several thousand ppm, especially Ti in DNP#01 and Cl in DNP#02. The results were summarized in Table. 1.

When DNP is placed directly under a neutron source as a reflector, the Wigner effect [1], a phenomenon in which a material is excited by radiation and its energy remains in the material for a long period of time, may be a problem in addition to impurities. The Wigner effect requires a longer irradiation time, but the results of this study suggest that the impurities that cause activation need to be reduced.

Table. 1. Contaminations in the DNP samples with unit of atom-ppm.

Impunity	DNP#01	DNP#02
Na	28	55
Cl	106	2042
Ti	287	12
Mn	1	9

Figure 1 shows a surface morphology of replica film (cellulose acetate) taken from sample without irradiation (left) and sample irradiated for 6 minutes. Although there are number of dots, which are probably due to aggregation of cellulose acetate molecule, the surface roughness values are 0.8nm and 0.63 nm in average, respectively. This indicate that irradiation of 2.6×10^{13}n/cm^2/s flux for 6 minutes does not affect the surface roughness of the mirror. The study of the impurities of NiP mirror by Gamma-ray spectra is under analysis.

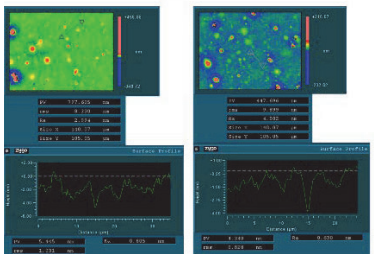

Fig. 1. surface morphology of replica film taken from NiP mirror without irradiation (left) and 6min irradiation (right).

REFERENCES:

[1] F. Cataldo *et al.*, Fuller. Nanotub. Carbon Nanostructures, **22:10** (2014) 861-865. (doi:) 10.1080/1536383X.2013.858131.